NASA TECHNICAL MEMORANDUM NASA TM-75725

THE STRUCTURE AND MICROPHYSICAL PROPERTIES OF THE CLOUDS OF VENUS

M. Ya. MAROV, V. Ye. LYSTSEV, V. N. LEBEDEV

Translation of "Struktura i mikrofizicheskiye svoistva oblakov Venery," (Academy of Sciences USSR, Institute of Applied Mathematics, Moscow, Preprint No. 144, 1978, pp 1-69

NATIONAL AERONAUTICS AND SPACE ADMINISTRATION
WASHINGTON, D.C. 20546 AUGUST 1979

THE STRUCTURE AND MICROPHYSICAL PROPERTIES OF THE CLOUDS OF VENUS

M. Ya. Marov, V. Ye. Lystsev, V. N. Lebedev
The Order of Lenin Institute of Applied Mathematics
im. Keldysh, USSR Academy of Sciences

Among the experiments carried out in the descent capsules /3* of the Venera 9 and 10 automatic stations, an important place was devoted to investigating the optical properties of the planet's atmosphere, including the study of the altitude distribution and the microphysical characteristics of the aerosols. For this purpose, identical sets of nephelometers were mounted in both capsules, by means of which the atmosphere of Venus was probed in two local regions separated by $\sim$ 2,000 km. Preliminary results from the analysis of the obtained experimental data have been previously published [8-9-10]. These were later refined with a consideration of a supplementary analysis on the technical and meteorological characteristics of the instruments and results of a parametric investigation of the aerosol models with respect to the procedure used in the experiment.

These investigations contain calculations by computer for the features of single scattering of non-polarized light by polydispersed spherical particles on the basis of the Mie theory, carried out by V.P. Shari and N.L. Lukashevich, for which these authors have developed special computer programs. Their description and the basic results of the calculations have been published in the form of IAM preprints numbers 83 and 105 for 1977 [6, 14]. These works also present examples for the calculated indicatrices in dependence on the determining parameters and their influence on the indicatrix of the scattering in the range of angles realized in the instrument complex was more thoroughly studied. The results of these calculations are

---

* Numbers in the margin indicate pagination in the foreign text.

presented in greater detail in [11].

Using the results of a more precise analysis, carried out by the authors, for an experiment based on these data, a model for the aerosol component in the Venusian atmosphere is considered. The main characteristics of this model are in good agreement with the earlier-published results. The authors express their gratitude to N.D. Rozman and L.D. Lomakina for their help in preparing the preprint.

I. The basic features of the nephelometer complex. /4

On the descent capsules of the automatic space stations Venera 9 and Venera 10, which landed on the surface of Venus on 22 and 25 October 1975, were mounted similar nephelometer complexes, consisting of two units: A small-angle nephelometer and a reverse-scattering nephelometer. Measurements were carried out during the descent of the capsule in the planetary atmosphere.

The nephelometer, being an optical instrument, is in the form of a photometer that measures the magnitude of the radiation φ_n, scattered by the medium under investigation (in the working chamber) and entering the photoreceiver tract. This magnitude can be compared with that of the originally emitted flux φ_0. The obtained ratios φ_n/φ_0 characterize the optical properties of the scattering media under investigation by means of the values for the coefficients of directional scattering.

Due to the specific nature of the physical conditions on Venus, the implementation of an optical experiment in its atmosphere from a space capsule required the surmounting of a number of technical and procedural difficulties. It was essential to develop instruments with acceptable characteristics in regard to weight and energy consumption. The limitations with respect to the information capacity of the radio link from

the vehicle to Earth required the development of a special procedure to reproduce the microphysical properties of the atmospheric aerosol with given unknown parameters by means of a minimum number of fixed angles to measure the scattering. The need to insure the working capability of the instruments in conditions of high temperature and pressure required the development of special means of heat protection. Further difficulties were due to the need to satisfy a high requirement as to static and dynamic strength (the G-factors upon entry of the descent capsule in the atmosphere of Venus attain $\sim$200 g). /5 A high reliability of the instruments was required, insuring their normal functioning at all stages of the test and after almost four months flight to Venus.

The spectral range for the operation of both units of the nephelometer complex was selected in the limits of 0.8-1.0 μm (at a level of 0.15) with an effective wave length $\bar{\lambda}$=0.92 μm. The first unit had fixed angles of 4.15° and 45° to measure the directional scattering with respect to the optical axis of the emitter, the fields of vision for the objectives being respectively 1° 10'x2° 20'; 2° 20'x 4° 50'; 6° 20'x 6° 20'. The divergence of the emitter beam was in the limits $\leqslant$ 2°. The angle between the optical axes of the photoreceiver and the emitter of the second unit was somewhat less than 180°, the distance between them was $\sim$ 90 mm, and the field of vision of the objective was $\sim$ 7°.

The nephelometer complex enabled the measurement of the ratio between the sounding flux φ_0 and the scattered (received) flux φ_n in the range of ratios φ_n/φ_0:

$0.8\cdot10^{-7} + 6.4\cdot10^{-6}$	for the angle 4° (channel #1)
$0.6\cdot10^{-7} + 5.0\cdot10^{-6}$	for the angle 15° (channel #2)
$0.2\cdot10^{-7} + 2.2\cdot10^{-6}$	for the angle 45° (channel #3)
$5\cdot10^{-8} + 10^{-6}$	for the angle 180° (channel #4)

During the process of descent in the atmosphere of Venus, the temperature rises up to ~740K and the pressure up to ~90 atm. Moreover, the ordinarily-used radio-electronic elements permit operation in considerably more moderate climatic conditions at a maximum temperature up to ~330°K and at normal pressure. Therefore the thermostatic control of the working chambers in the outer optico-electronic unit made use of a thorough multi-stage heat shield and thermal batteries that utilized the high specific heat of fusion of the working substance.

The thermal battery with elements of an electronic circuit /6 mounted inside was placed in a hermetically-sealed titanium body, calculated for a pressure of 100 atm, and was separated from it by a multi-layer heat insulation, filled with xenon. The choice of the working substance for the thermal battery was determined by the acceptable effective heat of fusion, with an allowance for the initial temperature of the internal compartment of the descent capsule, this latter being specially cooled prior to entry in the Venusian atmosphere down to a temperature of -5+or-10°C [1].

In consideration of these measures, the small-angle nephelometer preserved its working capability up to an environmental temperature of ~500°K and a pressure of ~10 atm and the reverse-scattering nephelometer up to a temperature of ~600°K and a pressure of ~100 atm. A diagram for the heat shield of the instrument, using the example of the reverse-scattering nephelometers, is shown in Figure 1.

To reduce the probability of possible distortions of the transmitted information in the units of the complex, there was a periodical calibration of the amplifier tract, automatically carried out every four minutes, which permitted an estimate for the level of internal and induced noise. There was also a system of signal processing to take into account the influence of external electromagnetic interference on the measurement results. A system to estimate the transmission coefficient of the optical

tracts and a system to measure the temperature in the outer optico-electronic units were also developed. The totality of these means of control significantly raised the reliability of the obtained experimental data and of their interpretation.

2. The sensitivity of the measurement channels.

The fundamental point in the creation of space-borne nephelometers is the choice of the requisite sensitivity of the measuring channels and their dynamic range. The absence of data as to the optical density, the structure, and the microphysical properties of the aerosol throughout the entire stratum of clouds (the determination of which is in fact the goal of the experiment) has admitted the possibility of varying these characteristics in rather wide bounds. /7

From an analysis of terrestrial polarimeter observations [15], estimates were obtained as to the mean effective size of the particles and the coefficient of refraction which, however, only referred to the upper limit of the clouds ($\tau \lesssim 2$-3). For the lower regions, the results of measurements as to the illumination in the automatic space station Venera-8 at an effective wave length of the receiver $\bar{\lambda} = 0.63$ μm [2] were very significant. For one of the most probable models of the cloud layer, a value of $\sigma \sim 3 \cdot 10^{-5}$ cm^{-1} for the space coefficient of scattering was obtained at $\tau \sim 50$ and the concentration of particles in a unit of volume was correspondingly estimated [5].

Taking these considerations into account, a range of instrument sensitivity was chosen that corresponds to a meteorological visibility within 0.05-1.0 km. In order to correlate the nephelometer characteristics to this range, calculations for the energy parameters and the optical circuit were carried out, along with experimental investigations on mock-ups in various types of fogs. In the development process, the sensitivity and range of the instruments were adjusted to a

meteorological visibility of 0.2-8.0 km.

a) The Energy Characteristics of a Small-Angle Nephelometer.

The intensity of non-polarized radiation $dI(\theta)$ (here and further on we consider a non-polarized monochromatic radiation with wave length λ), scattered by an elementary volume dV, illuminated by a parllel beam E_0, is equal to:

$$dJ(\theta)=E_0 dV \cdot \sigma \cdot \iota(\theta) \quad (1),$$

where σ is the space coefficient of scattering, $\iota(\theta)$ is the indicatrix of the scattering, standardized to 1, and θ is the angle between the direction of the incident and the scattered radiation. /8

Assuming that the elementary volumes are those formed by the geometry of the radiation beam and the field of vision of the photoreceiver, and considering the radiation beam to be parallel, the intensity of the scattering by these volumes can be written in the form:

$$J(\theta_j)=E_0 V_j \sigma \iota(\theta_j) \quad (2),$$

where j is the number of the measuring channel. Correspondingly these fluxes of the scattered radiation will be equal to:

$$\Phi_j=J(\theta_j)\omega_j=E_0 \sigma \iota(\theta_j) V_j \omega_j \quad (3),$$

where ω_j is the solid angle in which the scattering of the radiation is perceived by the photoreceiver. Expression (3), which is valid for small values of ω_j, can be rewritten in the form:

$$\Phi_j=E_0 S \sigma \iota(\theta_j) l_j \omega_j=\Phi_0 \sigma \iota(\theta_j) l_j \omega_j \quad (4),$$

where S is the normal cross section of the sounding light beam and l is the length of a ray in the beam that is located in the field of vision of the j-th photoreceiver.

Taking, for preliminary estimates of the aerosol characteristics, the values of the refractive coefficient, the effective particle size, and the width coefficient for the size distribution of the particles equal to $n = 1.45$, $r_3 = 0.75$ and 2.0 μm, and $\nu = 2$ ($n = m - i\varkappa$; $\varkappa \lesssim 10^{-3}$) respectively, we obtain the following value for the indicatrix $i(\theta_j)$: In channel 1 ($\theta = 4°$) $i_4 = 1.85$ and 6.2 steradians^{-1} ; in channel 2 ($\theta = 15°$) $i_{15} = 0.904$ and 0.467 steradians^{-1}; in channel 3 ($\theta = 45°$) $i_{45} = 0.101$ and 0.0855 steradians^{-1}.

Then for the region of values $\sigma = 10^{-5} + 10^{-4}$ cm^{-1}, the intensities of the fluxes of the scattered radiations are written in the following fashion:

$$\Phi_{n_1} = (7{,}2 \cdot 10^{-7} + 5 \cdot 10^{-6})\,\Phi_0$$

$$\Phi_{n_2} = (1{,}0 \cdot 10^{-7} + 2 \cdot 10^{-6})\,\Phi_0$$

$$\Phi_{n_3} = (3 \cdot 10^{-8} + 4 \cdot 10^{-7})\,\Phi_0$$

The obtained estimates permit the formulation of requirements for the sensitivity and dynamic range of each channel and to select the essential signal-noise ratio at the in-put of the amplifier that is determined by the expected minimum value of the scattered radiation flux $\Phi_{n_{3min}} = 3 \cdot 10^{-8}\Phi_0$. At the same time the power of the radiation source required to create the sounding flux Φ_0 and the field of vision for the photoreceivers is estimated. /9

b) The Energy Characteristics of the Reverse-Scattering Nephelometer.

The instrument has an infinitely-extended scattering volume, the contribution of its separate zones to the sensed flux of the scattered radiation not being equivalent and diminishing in proportion to the separation from the photoreceiver.

If we consider a portion of the scattering elementary volume with linear extent dx (Fig. 2), then the radiation flux scattered by this layer can be written, in approximation to single scattering, in the form:

$$d\Phi = A(x)\,\Phi_0\,\sigma\,\bar{i}_{\pi}\,dx\,e^{-2\sigma x} \qquad (5)$$

where $\bar{i}_{\pi}$ is a certain mean value for the scattering indicatrix in the layer dx in the range of observation angles and A(x) is a coefficient determined by the geometrical parameters of the instrument's optical circuit and characterizing the relative contribution of the portions of scattering volume.

If we assume that the radiation flux is uniformly distributed through the cross-section S, then:

$$A(x) \sim f(x) = \frac{S(x)}{S_0(x)}$$

where $S_0(x)$ is the cross-section of the light beam at a distance x_1 and S(x) is that portion of this section within the field of vision of the photoreceiver at a distance x. Obviously /10

$$f(x) = \begin{cases} 0 \text{ when } 0 \leqslant x \leqslant x_1 \\ 0 \div 1 \text{ when } x_1 < x < x_2 \\ 1 \text{ when } x \geqslant x_2 \end{cases}$$

In its turn, A(x) depends on the solid angle $\omega(x) = S'/x^2$, where S' is the area of the photoreceiver. The appearance of the function A(x), experimentally obtained, is shown in Figure 3.

The complete flux Φ_{π}, perceived by the photoreceiver, is obtained by integration of (5) with respect to an element of the sphere Ω in the direction of the normal to S':

$$\Phi_{\pi} = \int d\Phi = \Phi_0\,\sigma\,\bar{i}_{\pi} \int A(x)\,e^{-2\sigma x}\,dx \qquad (6)$$

the calculation of $\int A(x)\,e^{-2\sigma x}\,dx$ has shown: 97% of the received scattered radiation arrives from a zone with $x \leqslant 20$ m. The factor $e^{-2\sigma x}$ in the limits of the expected values of σ practically does not influence the values of the integral (6). For an instrument realized in practice

$$\int A(x)\, e^{-2\sigma x}\, dx = 0.372 \text{ cm} \cdot \text{steradians}$$

Estimates for the magnitude of the flux φ_n were done by using $\bar{i}$ values that, as in the case of the small-angle nephelometer, are determined from calculation of the scattering indicatrices for aerosols with n = 1.45, r_3 = 0.75-2.0 μm, and ν = 2 for λ = 0.92 μm.

With an allowance for the instrument geometry, the averaging of i values was done in the interval 174-180°, the i_{180} values being equal to 0.025-0.055 steradians $^{-1}$. In the range $\sigma = 10^{-5}$ 10^{-4} cm^{-1} we obtain:

$$\Phi_n = \Phi_0 (9 \cdot 10^{-8} + 2 \cdot 10^{-6})$$

The basic energy characteristics of the instrument were chosen with a regard to the above. In the process of its fabrication and graduation, they were rendered even more precise.

3. The Influence of the Parameters of the Complex' Optical Circuits on the Measurement Results.

/11

In the general case, when solving inverse problems of light scattering, rather strict requirements are imposed on the radiation's monochromaticity, the divergence of the light beams and the magnitude of the angles of vision for the receivers and emitters, the accuracy of the photometric evaluation, and the volume of measurement information. In practice, however, instruments are built that have perceptible deviations from the ideal circuits and instrument errors. Thus the initial data (the measurement results) usually contain errors that frequently impede the interpretation of the approximate solution that is produced.

The basis of the method that was realized in the space-borne nephelometer complex is the existence of a correlation between the coefficient of the directed scattering at the 4th values of

the scattering angles θ_j and their relationship with such characteristics of polydispersed systems of spherical particles as the mean or effective particle size, the width of the distribution, the concentration of the particles, and the index of refraction. Preliminary theoretical estimates enabled the finding of a region of angular vàles and wave lengths, within which the existence of such a correlation is most characteristic and enables a reconstruction of the particle spectrum with various distribution parameters. In this case, the requirements as to monochromaticity and divergence of the beams are considerably relaxed, and it is only necessary to know the spectral characteristics of the receiving-transmitting optical tract $F(\lambda)$ and the distribution for the intensity of the scattered radiation with respect to the scattering angles, determined by the weighting function $f_j(\theta)$ for each of the measuring channels.

The physical meaning of the weighting function consists in the fact that it describes the relative distribution (directionality diagram) of the scattered radiation perceived by the photoreceiver with respect to the scattering angle in the case of a spherical indicatrix of the scattering medium. For convenience in using /12 these functions we shall introduce their normalization condition:

$$\int_{\lambda_1}^{\lambda_2} F(\lambda)\,d\lambda = 1, \qquad \int_{\theta_{j1}}^{\theta_{j2}} f_j(\theta)\,d\theta = 1 \tag{7}$$

where λ_1 and λ_2 determine the width of the radiation spectrum and θ_{j1} and θ_{j2} are the extreme angles for the scattering in each of the measuring channels. Now, there will correspond to the measurement results certain effective values for the index of directional scattering, determined by the relationship:

$$\bar{\sigma}(\theta_j) = \int_{\lambda_1}^{\lambda_2}\int_{\theta_{j1}}^{\theta_{j2}} \sigma(\lambda,\theta) F(\lambda) f_j(\theta)\,d\theta\,d\lambda = \int_{\lambda_1}^{\lambda_2}\int_{\theta_{j1}}^{\theta_{j2}} \sigma(\lambda) L(\lambda,\theta) F(\lambda) f_j(\theta)\,d\theta\,d\lambda \tag{8}$$

where $\sigma(\lambda,\theta)$ is the index of directional scattering, $\sigma(\lambda)$ is the space coefficient (index) of the scattering, and $i(\lambda,\theta)$ is the scattering indicatrix, normalized for 1. The process of modeling $\bar{\sigma}(\theta_j)$ and the interpretation of the experimental data for this approach are considerably complicated. To simplify the measurement interpretation, when developing the apparatus it was essential to satisfy the condition of quasi-monochromaticity of the radiation, which can be written in the form:

$$\frac{\varphi(\bar{\lambda})-\int_{\lambda_1}^{\lambda_2}\varphi(\lambda)F(\lambda)\,d\lambda}{\varphi(\bar{\lambda})}\leqslant\delta_M \qquad (9)$$

where $\varphi(\lambda)$ is the scattering function and $\bar{\lambda}$ is the effective wave length of the radiation. In other words, the values of the scattering function at an effective wave length of $\bar{\lambda}$ should not differ from the mean value by more than a given error δ_M in the entire class of possible structures that are considered. The spectral characteristics of the receiving-transmitting tract of the space-borne nephelometer complex are included in the wave length range λ = 0.85-1.0 μm at $\bar{\lambda}$ = 0.92 μm, so that the magnitude of δ_M does not exceed 1-2%. According to the results of a numerical integration, the chosen form of the dependence $F(\lambda)$ insures the satisfaction of condition (9). /1

Relation (8) can then be rewritten in the form:

$$\bar{\sigma}(\theta_j)=\int_{\theta_{j1}}^{\theta_{j2}}\sigma(\bar{\lambda})i(\bar{\lambda},\theta)f_j(\theta)\,d\theta=\sigma\int_{\theta_{j1}}^{\theta_{j2}}i(\theta)f_j(\theta)\,d\theta=\sigma\bar{i}(\theta_j) \qquad (10)$$

where $\bar{i}(\theta_j)$ and $\bar{\sigma}$ are the effective values of the indicatrix and the space coefficient (index) of scattering for $\bar{\lambda}$ = 0.92 μm. As the experimental determination of weighting functions is difficult, the functions $f_j(\theta)$ for all the channels of the nephelometer complex were determined by calculation, starting with an analysis of the parameters for the optical circuits.

The distribution of the radiation sources' brightness with respect to the luminous body was experimentally determined.

The appearance of the weighting function is shown in Figures 4 and 5. The influence of these functions on the measurement results can be shown by Table 1, which presents the values of the scattering indicatrix $i(\theta_j)$ at θ_j = 4°, 15°, 45°, and 180° and the effective values of $\bar{i}(\theta_j)$ for models of polydispersed non-absorbing aerosols ($\varkappa = 0$), having a Gamma-distribution of particles with respect to size and the following characteristics: n = 1.33 and 1.45, τ_3 = 0.5, 2, and 6 μm, and μ = 2 and 12.

It follows from Table 1 that, in the 15° and 45° channels, the weighting functions exert a weak influence on the measurement results. The difference between $i(\theta_j)$ and $\bar{i}(\theta_j)$ is not more than 2%, whereas it may attain 15-25% for the 4° and 180° channels.

Table 1.

Значения а. характеристик				4°		15°		45°		180°	
n	$\varkappa$	τ_3	μ	i	$\bar{i}$	i	$\bar{i}$	i	$\bar{i}$	i	$\bar{i}$
I,45	0	0,5	2	I,3	I,29	0,860	0,856	0,II4	0,II5	0,0I76	0,0I69
I,45	0	0,5	I2	I,I7	I,I6	0,867	0,86I	0,III	0,II2	0,0I46	0,0I43
I,45	0	2	2	6,25	5,88	0,547	0,543	0,087	0,087	0,0556	0,0462
I,45	0	2	I2	6,84	6,5I	0,468	0,468	0,080	0,080	0,0570	0,0450
I,45	0	6	2	6,I	5,46	0,390	0,385	0,080	0,08I	0,0720	0,0770
I,45	0	6	I2	5,52	4,89	0,380	0,365	0,080	0,08I	0,0730	0,0830
I,33	0	0,5	2	I,59	I,58	I,000	0,960	0,099	0,I00	0,0090	0,0089
I,33	0	2	2	6,34	5,97	0,646	0,640	0,079	0,080	0,04I3	0,0324
I,33	0	6	2	6,3	5,66	0,492	0,488	0,067	0,068	0,0470	0,0370

Key: a, values of the characteristics. (Note: Commas in tabulated material are equivalent to decimal points).

Thus, the weighting functions in the measuring channels, /14

which take into account the actual geometry of the light beam, are a source of error in determining the indices of the directional light scattering during the measurements, since the measured values of $\bar{\sigma}(\theta_j)$ may differ considerably from $\sigma(\theta_j)$ in dependence on the properties of the aerosols. A calculation of the function $f_j(\theta)$ when modeling the measurement results for $\bar{\sigma}(\theta_j)$ allows this error to be almost completely eliminated.

We shall discuss yet another possible source of error in the determination of $\sigma(\theta)$, connected with the calculation of radiation attenuation in the tract emitter-scattering-volume-photoreceiver.

As was already mentioned in Section 2, calculations for the dependence (6) show that $\int A(x) \cdot e^{-2\alpha x} dx = \int A(x)\, dx$ in the entire range of σ values that are of interest; consequently it is possible to disregard the attenuation of the radiation when processing the measurement data. For the 4°, 15°, and 45° channels, this assertion is even more valid since the measurement base of these channels is much less and is found within the limits of 400 mm. /15 Thus, considering the stipulated features of the method that was used, we can to a first approximation, and without detriment to the accuracy of the interpretation for the experimental data, consider the magnitude of the above-discussed errors to be close to zero.

4. The Procedure and Results of the Graduation

The output signals of the complex' measuring channels, developed in the form of a constant potential u_j within the bounds 0-6.3 V, depend on the flux φ_{n_j} of the scattered radiation perceived by the photoreceiver, which is linearly correlated with the effective value of the index of directional scattering $\bar{\sigma}(\theta_j)$. Correspondingly, the calibration characteristics of the channels are in the form of the dependence

$$U_i = f[\bar{\sigma}(\theta_i)] \qquad (11)$$

For the calibration of the nephelometers, the following procedure was developed, intended to specify and control the photometric characteristics of the instruments primarily in laboratory conditions:

a) Typical calibration characteristics (11) were obtained on the base of an energy calculation and a full-scale graduation of nephelometer mock-ups in aerosol media;

b) At a number of points on the obtained calibration dependences, the relationship between the emitted Φ_0 and the scattered Φ_n fluxes was established. The resulting photometric characteristics $U_j = f[\Phi_{n_j}/\Phi_0]$ (12) were considered as a reference and, with a given accuracy, were transferred to the entire set of instruments by means of special graduating devices (cf. Section 5);

c) Individual series models of both nephelometers were again calibrated in aerosol media for the purpose of refining the typical calibration dependences (11); /16

d) By means of the photometric dependences (12), rated for each instrument, the individual calibration characteristics (11) were determined.

This procedure enabled the calibration of the nephelometers with a minimum expense of time and facilities.

The calibration characteristics (11) can be obtained in principal by various methods:

- The analytical method, wherein the calibration characteristics are computed from the initial parameters of the optical circuits, taking into account the spectral characteristics of the source and receiver of the radiation and of the elements of the optical circuits, as well as the characteristics for transforming the received flux of scattered radiation into the output electrical signal;

- The method of a standard medium, which consists in the implementation of measurements by an instrument in a medium with a previously-known indicatrix and index of scattering;

- The method of a controlled indicatrix, wherein the calibration is carried out in an arbitrary scattering medium with simultaneous measurements by the instruments being calibrated and by a control meter of the indicatrix.

None of these methods was capable of realization in the practical solution of the problem of calibrating the nephelometer complex; thus, the following the method was proposed and realized. In a polydispersed medium, consisting of spherical particles of a known nature, there were carried out simultaneously /17
measurements by the instruments to be calibrated and measurements on the microstructure of the aerosols by means of a control apparatus. The measurement data as to the microstructure were used to calculate the scattering functions $i(\theta)$ and σ . Then, by formula (10), the effective values of $\bar{\sigma}(\theta_j)$, corresponding to the moments of the measurements, were determined.

Water aerosols at positive temperatures were chosen as the working medium . They were produced in a large aerosol chamber at the Institute of Experimental Meteorology (IEM) [4]. The chamber was equipped with instruments to measure the temperature and pressure as well as means to measure the transparency of the fog and its microstructural characteristics. The measure of the concentration and size distribution of the fog droplets was implemented by means of the "Aelit" photoelectrical counter and a ten-channel amplitude analyzer, both developed at the IEM. Before each series of readings, a control calibration of the "Aelit" was carried out by means of a sedimentometer. In this operation, the time for aspirating the medium through a capillary was 0.5 sec and the rate of draw was ~ 2 cm^3/sec. A single analysis of the fog microstructure was made from a volume of 1 cm^3.

As a result of processing the measurement results, the concentration N of the droplets, the normalized size distribution of the droplets, the arithmetic mean, root-mean-square, and root-mean-cube radii of the droplets r_1, r_2, and r_3, and the attenuation index of the medium $\alpha = 2\pi r_2^2 N$ were determined. If the distribution of droplets is approximated by a Gamma-distribution, then the processing program enabled a determination of the parameter μ and the modal radius of the particles r_0.

For the purpose of an additional control as to the correctness of the microstructure measurement, parallel measurements were made as to the transparency of the fog by a single-channel reference photometer of direct action. The range of α values in the fogs was α = 0.01-0.3 m^{-1}, during the graduation. /18

Depending on the mode of pressure release in the chamber when creating the artificial fog, each test lasted from 3 min to 3 hours. In all, ten tests were carried out. In the course of each test, as the fog was breaking up, a continuous registration of the signals from the instruments being calibrated and the transparency meter was made. The measurements for concentration and size distribution of the droplets was done once a minute.

To construct the calibration characteristics of the nephelometers from a large volume of obtained experimental material, a consecutive sampling of the primary measurement data was done. In the beginning, measurements were sampled in separate periods of time, in the course of which all of the measured values $\alpha_{meas.}$ were close to the calculated values $\alpha_{cal.}$ obtained from measurements of the microstructure; afterwards measurements were samples within these intervals, when the function of the size distribution for the droplets was approximated by a Gamma-distribution. As a result, approximately 50 points were obtained to construct the calibration characteristics of each channel.

The measurement data on the microstructure and transparency of the water aerosols were used to calculate $i(\theta)$ and $\alpha \simeq \sigma$, and formula (10) was used to calculate $\bar{\sigma}(\theta_j)$. To the calculated values of $\bar{\sigma}(\theta_j)$ there were matched magnitudes u_j of signals at the output of the measuring channels at the same moments of time. As a result, for each of the channels there was obtained a field of points and, by the method of least squares, calibration characteristics corresponding to the dependence (11) were calculated. The shape of these characteristics was determined with an allowance for the rated photometric characteristics (12) which, for the entire working segment, were in the form of straight lines. The root-mean-square deviation of individual points from the approximating calibration lines was: For the 4° and 15° channels $\delta_u^{\varphi} = +15\%$; for the 45° channels $\delta_u^{\varphi} = +20\%$; for the 180° channels $\delta_u^{\varphi} = +10\%$. /19

5. The Instrument Error of the Measurements

To obtain reliable information as to a measured parameter it is essential to make a correct allowance for the errors that arise during calibration, photometric evaluation, and transmission of the information, as well as the influence of destabilizing factors since, as has already been remarked, when operating in the atmosphere of Venus the instruments are subjected to the action of high temperature and pressure, mechanical loads, optical and electromagnetic interference, et cetera. It is thus necessary to establish primarily the instrument error of the device, which influences the actual value of the measured magnitude φ_n.

The magnitude of the output potential u_j, depending on the intensity of the flux of scattered radiation as per (11), is determined by the sensititivy of the receivers and the parameters of the amplifiers, the energy characteristics of the emitters (associated with the operating conditions), interfering physical conditions in the environment, et cetera. All of these distort

the true relationship between the measured output potential and the magnitude of the scattered radiation flux.

The instrument error δ_u of the measurements is comprised of the following basic components:

$\delta_u^{ph.}$ - the error in determining the natural photometric curve of the instrument,

δ_u^{φ} - the calibration error in aerosol media,

$\delta_u^{cl.}$ - the climatic error,

$\delta_u^{c.}$ - the convergence of the instrument reading,

$\delta_u^{b.}$ - the error introduced by background radiations, internal noise, and transient instability,

$\delta_u^{\tau.}$ - the error of the telemetry system. /20

We shall consider these components more closely and shall analyze their relative contribution to δ_u.

a) The output photometric characteristics and the errors $\delta_u^{ph.}$ and δ_u^{φ}. When calibrating photometric instruments the simplest and most accessible method is that in which the final result, expressed in the attenuation of the sounding radiation flux, is simulated. For this purpose various types of attenuators in the form of filters, mirrors, diaphragms, etc., are usually employed. Neutral light filters or diaphragms are used more frequently.

In the process of determining the photometric characteristics, the dependnece of the output potential on a consecutive series of ratios for the received light flux φ_n to the radiated flux φ_0 should be determined. This may be done by using a special attachment that provides for a reduction of the light flux with respect to the original magnitude by several orders and a directed arrival of the attenuated light flux successively at each channel. Such an attachment should also possess the necessary rigidity of structure and fixation of its basic element,

so as to reduce the error of the operation.

Diagrams of the attachments used to calibrate small-angle and reverse-scattering nephelometers are shown in Figures 6 and 7, respectively. The requisite total calibrated attenuation of the flux is attained by means of an assembly of neutral attenuators, diaphragms and mirrors (or screens in the diagram in Figure 7). The operation of determining and correcting the photometric characteristics is done in several stages in difference climatic conditions, the other factors of influence being varied. Figure 8 shows a typical dependence of the output potential on the magnitude of φ_n / φ_0 for one of the small-angle nephelometers (the output of the synchronous detector of the 4[a] channel). /21

The error in determining the photometric characteristics of the instruments is specified by the error in the certification the principal standard measures assumed for the calibration: The light filters and the specimens of a white reflecting surface. This error is within the limits of 0.5-1% with respect to the maximum of transmission or reflections. The attachments and their parts are usually certified at the level of error of the measuring facilities used for the transformation and registration of the output signals. The total error of the photometric evaluation is specified in this case on the basis of a calculation with respect to all the individual units and its magnitude depends on the quantity of these units and the error of their certification. It is ± 2.5% for the small-angle nephelometer and ± 1.5% for the reverse-scattering nephelometer. It is to be noted that these magnitudes do not include the errors introduced by the constant element of the calibrating device -- the mirrors, diaphragms, lenses, and screens. These errors are systematic and common for all instruments. The magnitudes of the error δ_u^{φ} are indicated in section 4.

b) The convergence of the instrument reading and the

supplementary (climatic) error (δ_u^c and δ_u^{cL}). The convergence of the readings, i.e., the quality that characterizes the nearness of the random instrument errors to zero, is on the average δ_u^c ± 5% in the entire dynamic range in normal conditions. The supplementary errors, manifested in the distortion of the natural photometric dependence of the instrument, arise due to the changing conditions of the environment, most of all temperature changes. In the experiments aboard the Venera-9 and Venera-10, the atmospheric temperature changed from 0 to +220° C for the small-angle and from 0 to +360° C for the reverse-scattering nephelometer. For the actual rise in temperature of the individual instrument assemblies during the descent in the atmosphere, and proceeding from the results of the calibration, the estimated limiting values of the error (in percentages) are shown in Table 2. /22

TABLE 2.

	a. Венера-9				b. Венера-10			
c. Канал θ_j	4°	15°	45°	180°	4°	15°	45°	180°
$\delta_u^{ц}$, %	2	2	10	10	0	1	9	15

Key: a, Venera-9; b, Venera-10; c, θ_j channels.

c) The telemetry error. The error introduced by the telemetry system is composed of the transformation error (the error that arises during the computing, transformation, and transmission of the information) and the error due to the discreteness of the information transmission. Figure 9 shows the absolute magnitude for the telemetry error as a factor of the output signal potential. Table 3 presents a statistical analysis of the voltage distribution for the output signals of the instruments in percentages, obtained in the experiment.

TABLE 2. The Number of $U_{out.}$ Values, in Percent

Выходные сигналы a, $U_{вых}$;	c Венера-9				d Венера-10			
	Каналы: 4° b.	I5°	45°	I80°	4°	I5°	45°	I80°
0,I-0,5	I4,3	37,5	22,3	-	-	-	-	-
0,5-I,0	20,7	I0,7	I5,3	I,3	0,66	7,9	I,3	I,I
I-2	20,7	5I,3	55,4	22	29,6	75,6	56,6	8,8
2-3	35	0,4	6,9	24,4	25,6	II,2	40,I	I8,3
3-4	9,3	-	-	I5,7	35,5	3,3	2,0	27,4
4-5	-	-	-	I6,3	8,5	I,9	-	28,6
5-6,3	-	-	-	20,3	-	-	-	I5,7

Key: a, output signals; b, channels; c, Venera 9; d, Venera 10. (Note: commas in the tabulated material are equivalent to decimals).

From a comparison of Figure 9 and Table 3 it is evident that the main portion of the obtained data has an error $\delta_u^{\tau} \lesssim 2.5\%$.

d) The errors introduced by background noise, internal noise, /23 and instability of the instrument characteristics with regard to time δ_u^{β}. The background noise, acting on the photoreceivers, can produce a distortion of the obtained information. Depending on the nature of the background interference, the design features of the instruments, and the magnitude of the useful signal, the measurement results can be understated or exaggerated. The mechanism and the degree of action of the background noise on the specific type of photometric instruments are poorly amenable to theoretical analysis and it is most easy to estimate its contribution by the results of special laboratory experiments. Such experiments show that the sensitivity of the space-borne nephelometers is practically invariant at constant background noises up to $7.5 \cdot 10^4$ lux. To protect the photoreceivers from the large background noises that are present at the level of the

upper cloud boundary, a number of design measures is provided in the instruments.

The error introduced by the internal noises of the electronic circuits can influence the measurement results only if the useful signal happens to be at the level of the instrument's internal noises. The influence of various electromagnetic (optical or electrical) interferences, penetrating to the amplifier and causing in the end an increase in the noises at the instrument output and, as a consequence, a contraction of the dynamic range and a loss or distortion of information, should also be attributed to this cause. The design of the space-borne nephelometers enabled a determination of the presence and level of noises (interference) during the operation of the instrument and allowed them to be taken into account during the processing. In the experiments aboard the Venera-9 and Venera-10, no surpassing of the permissible level of noise was detected.

Considering that the total operating time of the instruments from the moment of their preparation to the carrying out of the experiment does not exceed 10 hours, while the time for storage and transportation to Venus is approximately 10 months all together, the change in the instrument characteristics due to aging of the elements is insignificant. An investigation of one of the instruments, similar to those mounted aboard the Venera-9 and Venera-10, did not reveal any change in the characteristics a year after fabrication. /24

Thus, we may conclude that the errors introduced by background noises, internal noises, and instrument instability with respect to time are insignificant and can be disregarded, $\delta_u^{\theta} \simeq 0$. By now considering the errors discussed in sections a) - e) as non-correlated random variables, we can determine the total instrument error of the measurements for $\bar{\sigma}(\theta_j)$ in the nephelometer measuring channels as:

$$\delta_u = \sqrt{(\delta_u^{\theta})^2 + (\delta_u^{\varphi})^2 + (\delta_u^{c})^2 + (\delta_u^{T})^2}$$

A calculation gives $\delta_u \lesssim 19\%$. The other components of the instrument error, being systematic, are taken into account when processing the obtained data.

6. The Procedure for Interpreting the Measurement Data.

The determination of a medium's microphysical properties by the measured characteristics of the radiation, scattered by this medium, is an example of a situation in which relatively slight measurement errors can lead to arbitrarily large changes in the solution. As is known, such problems belong to the class of improperly stated problems.

In our particular problem there is limited information as to the index of scattering in four directions. For this reason, speaking in general, it is difficult to use here the known methods for solving inverse problems, such as the method of fitting or quasi-solution, which, for the equation $Az = u$, uses initial data of u for solution elements $\tilde{z}$ from the set of M ($u \in U$, $z \in F$, $U \subset F$ being metric spaces, A is an operator that transforms F onto U) to search for the minimum of the functional /25
$S_\nu(Az,u) = \inf_{z \in M} \rho_\nu(Az,u)$ [13]. At a given stage we made use of a simplified variant of the fitting method. Taking a broad class of possible structures (elements $M \subset F$, dependent on a finite number of parameters), we calculated the physical fields corresponding to them and, comparing them with the results u of the measurements, belonging to the space of U, selected as solution the most suitable (or "permissible") structure. The minimization of the discrepancy $\rho_\nu(Az,u)$, strictly speaking, is done either approximately or not at all. This method is completely effective and, as numerical experiments on the study of light scattering characteristics have shown (6), assuming a definite law for the

size distribution of the aerosol particles, it is possible to obtain sufficiently reliable estimates for the generalized characteristics of the aerosol structure, viz., the mean size and concentration of the particles, the width of the distribution, as well as the index of refraction, from a measurement of scattering in four directions. The investigations were carried out for a sufficiently broad class of possible atmospheric aerosol structures.

For the analysis we chose a Gamma-distribution for the particles with respect to size as being the most frequently encountered type of approximation to actual distribution:

$$n(r)=A\cdot r^{\mu}\cdot e^{-\mu\frac{r}{r_0}}=A\cdot r^{\mu}e^{-\frac{\mu+1}{r_e}\cdot r} \qquad (13)$$

where A is the normalizing factor, μ is the parameter for the width of the distribution, r_0 is the modal radius, and r_e is the effective radius of the particles, determined by the relation

$$r_e=\frac{\int r^3 n(r)\,dr}{\int r^2 n(r)\,dr} \qquad (14)$$

For the normalization condition $\int n(r)\,dr=1$, the value of the normalizing factor is equal to: /26

$$A=\frac{(\mu+3)^{\mu+1}}{\mu!\,r_e^{\mu}}$$

this size distribution law for the particles is usually realized in terrestrial clouds and is also employed in interpreting the results of Earth-based polarimitry observations of Venus [15]. Furthermore, it is known from a number of works (cf., e.g., [12]) that, when $r_e \geqslant 1$ μm, for various types of distributions and in particular for the normal-logarithmic and the Gamma-distribution, the scattering characteristics become practically identical for the same values of the effective particle size and the width of

the distribution.

Calculations for the scattering indicatrices were carried out for aerosol structures in the ranges of values: $z_e = 0.1 + 6.0$ μm, $\mu = 1 + 20$, $n = 1.33 + 2.0$, $\varkappa = 0 + 1.0$ [14]. The choice of the node values for the parameters of this four-dimensional network was conditioned by the problem, on the one hand, of reducing to a minimum the volume of extended calculations and, on the other hand, of obtaining values for the scattering characteristics with a calculation step that uses parameters that enable a continuous interpolation. In all, approximately 400 scattering indicatrices were calculated at values for the scattering angles θ° = 2(0.5)7, 12(1)18, 40(1)50, 170(1)180 [11].

After this, using the data from the calculations for the scattering indicatrices $i(\theta)$, the values of $\bar{i}(\theta_j)$ were calculated in conformity with formula (10), as were the relations

$$f_1 = \frac{\bar{i}(4°)}{\bar{i}(15°)}, \quad f_2 = \frac{\bar{i}(4°)}{\bar{i}(45°)}, \quad f_3 = \frac{\bar{i}(180°)}{\bar{i}(45°)} \qquad (15)$$

On this basis, families of nomograms, reflecting the correlation of the scattering indicatrix parameters $f_{1,2,3}$ with the microphysical characteristics of polydispersed system of spherical particles z_e, μ, n, and $\varkappa$, were constructed, the wave length of the sounding radiation being $\bar{\lambda} = 0.92\,\mu$m. We note that the obtained regularities preserve their force even for other values of λ, /27 since, instead of z_e, it is possible to introduce the non-dimensional parameter ρ_e (the relative particle size, used in the theory of Mie), associated with z_e by the relationship $\rho_e = \frac{2\pi z_e}{\lambda}$.

We shall analyze these regularities and, at the same time, determine the bounds of the capabilities of our method.

The dependence of f_1 on ℓ_e (Fig. 10) is represented by an abruptly increasing function in the size range 0.5-3 μm and there exists a zone of poor sensitivity to ℓ_e for 0.5 μm $< \ell_e <$ 3 μm. For $\ell_e \gtrsim 4$ μm, f_1 becomes a diminishing function.

The dependence of f_1 on μ (Fig. 11) is poorly expressed. For small particles ($\ell_e \lesssim 1$ μm), f_1 is a predominantly diminishing function that rises for larger particles, beginning with $\ell_e \gtrsim 1$ μm. There is practically no dependence for f_1 on the index of refraction within the limits of real values for both actual (m = 1.33-1.6) and imaginary ($\varkappa < 10^{-3}$) components (Fig. 12, 13).

The function $f_2(\ell_3)$ also has an abruptly increasing character at first, but already attains its maximum in the range $\ell_e \simeq$ 0.2-3.0 μm and becomes a diminishing function at $\ell_e \gtrsim 3.5$ μm (Fig. 14). The dependence of f_2 on μ is also poorly expressed. At the same time, the dependence of f_2 on n and $\varkappa$ becomes more pronounced. Thus, at $\ell_e \lesssim 1$ μm, $f_2(n)$ is an obviously decreasing function (Fig. 15), while the dependence of f_2 on $\varkappa$ has a linear nature with a somewhat larger tangent for the angle of inclination than that of f_1. Nonetheless, within the limits of real values $\varkappa = 0 + 3 \cdot 10^{-3}$, the relative change of f_2 does not exceed ~15%.

The functions f_3 are correlated with the microphysical characteristics in a more complicated fashion. Within the limits ℓ_e = 0.5-1.5 μm, $f_3(\ell_e)$ is a predominantly increasing function (Fig. 16), its slope depending considerably on n. In the interval ℓ_e = 1.5 + 2 μm, as n changes from 1.33 to 1.5, $f_3(\ell_e)$ is converted from an increasing to a decreasing function (Fig. 17). /28
In the interval ℓ_e = 2 + 3 μm, there exists a zone of insensitivity for both $f_3(\ell_e)$ and $f_3(n)$. The dependence of $f_3(\mu)$ is poorly expressed and is only an increasing function for $\ell_e \simeq 1.5$ μm. Depending on the coefficient of absorption, the function $f_3(\varkappa)$ is monotonic decreasing, but in the range of values $\varkappa = 0$ to $3 \cdot 10^{-3}$, its change is insignificant and is approximately ~20-30%.

From the nature of the dependences of the functions f_1, f_2, and f_3 on r_e, μ, n, and $\varkappa$, there follows a number of conclusion that served as the foundation for the procedure of estimating the characteristics of the investigated aerosols by limited measurement data, as well as certain qualitative criteria for the uniqueness of the results of the estimates:

1. It is expedient to use the values of the functions f_1 and f_2 to obtain estimates for the characteristic (effective) size r_e and the parameter μ. In this case, the substantial discrepancy of the r_e estimates by f_1 and f_2 as the parameter μ varies may testify to the deviation from the Gamma-distribution of the size distribution for the particles of the investigated medium. The determination of the parameter for the width of the distribution μ can be carried out approximately, with only an indication of the range of μ values, e.g. 1-2 or 8-20.

2. An estimate of the real part of the refractive index n for $r_e \leqslant 1.5\text{-}2\ \mu$m is chiefly determined by the value of f_3, since this function depends on n to a considerably larger extent and on r_e to a lesser extent than do f_1 and f_2. For $r_e \gg 1.5\ \mu$m, the estimates for n become less determinate. As to the imaginary part of the refractive index, the ordinary atmospheric aerosols at $\lambda \simeq 0.9\ \mu$m have a slight actual absorption, $\varkappa \lesssim 3 \cdot 10^{-3}$. With regard to the atmosphere of Venus, this assertion is apparently still valid at least for the upper portion of the cloud layer [15]. /29
At such values, the absorption has a weak influence on f_1, f_2 and f_3 and thus we may practically eliminate this parameter from future consideration.

3. As can be seen from Figures 10 and 14, functions f_1 and f_2 in a certain region of values may give ambiguous estimates for r_e: Either $r_e \lesssim 3\ \mu$m or $r_e > 4\ \mu$m. The value of f_3 may serve as a certain qualitative criterion for the selection of one or the other range of r_e since, as a rule, for $r_e < 3\ \mu$m it is less or much less than the value of f_3 for $r_e > 4\ \mu$m.

4. The accuracy of the estimates for λ_e, μ, and n is determined by both the instrument error of the measurement for f_1, f_2 and f_3, and by the specific regions of values for the characteristics being estimated. Thus, for example, when λ_e = 0.5-1.5 μm, the refractive index n in the interval of values 1.4-1.5 can be estimated by the results of measurements for f_3 with an accuracy to ± 0.01 for an instrument error up to 15%, whereas for values $\lambda_e \simeq$ 1.5-3.5 μm, the estimate of n involves great difficulty even at a higher accuracy of measurements.

In consideration of criteria 1-4, the following procedure for interpreting the experimental data was accepted:

- using the results of measurements by the space-borne nephelometer complex in the investigated medium, the values of $\sigma(\theta_j)$ at the moment of time t, corresponding to a height h above the surface of the planet, are determined and the experimental values for the functions f_1, f_2, and f_3 are calculated;

- using the families of nomograms, and with the parameters μ and n varying, they are identified with calculated values for f_1, f_2, and f_3, in this way the models giving the best coincidence for λ_e estimates being sought;

- the error in the determination of λ_e, n, and μ is estimated; /30

- the uniqueness for the determination of the values for the aerosol characteristics is qualitatively evaluated;

- using the assumed models for the investigated aerosol, the coefficient of scattering σ, the concentration of particles N, and the optical thickness T of the aerosol layer are calculated.

The scattering coefficient is determined from relation (10):

$$\sigma(h)=\frac{\bar{\delta}_{\theta_j}(h)}{i(\theta_j,h)} \qquad (16)$$

where $i(\theta_j,h)$ is determined according to the data of model calculations

$$i(\theta_j,\tau_a,n,\varkappa,\mu).$$

The optical thickness of the layer h_0-h of aerosols, where h_0 is the altitude that corresponds to the beginning of measurements, is found by a numerical integration in accordance with the relation:

$$\tau=\int^{h_0}\sigma(h')\,dh' \qquad (17)$$

The concentration of particles N is associated with the scattering coefficient σ by the relationship:

$$\sigma=N\bar{F}_\lambda(n,\tau_a,\mu)\cdot\pi\frac{(\mu+1)(\mu+2)}{(\mu+3)^2}\tau_a^2 \qquad (18)$$

where $\bar{F}_\lambda(n,\tau_a,\mu)$ is the average factor for the effectiveness of scattering, determined by the identity:

$$\bar{F}_\lambda(n,\tau_a,\mu)=\frac{\int F_\lambda(n,r)\,\pi r^2 n(r)\,dr}{\int \pi r^2 n(r)\,dr} \qquad (19)$$

Calculations of $\bar{F}_\lambda(n,\tau_a,\mu)$ for a number of aerosol models are shown in Table 4.

TABLE 4

$n(\mu=2)$			ρ_e	τ_3 (at m) $\lambda=0,92$ m
I,33	I,45	2,00		
2.8	3.05	2.67	5.I	0.75
2.9I	2.79	2.48	7.7	I.I2
2.77	2.64	2.5I	9.5	I.40
2.48	2.42	2.37	I4.I	2.I0
2.34	2.3I	2.28	I8.8	2.80

7. Results of the Nephelometer Experiment in the Atmosphere of Venus.

During the time of operation in the atmosphere of Venus, approximately 6,520 binary units of information were transmitted to Earth through the telemetry channels from the set of instruments of the Venera-9 station and approximately 5,280 binary units from the set aboard the Venera-10. As a result of their primary processing, discrete values were obtained for the constant potential at the output of the measuring channels in dependence on the time, $U_j(t)$, and, in accordance with the calibration characteristics (11), the values of $\bar{\sigma}_{\theta_j}(t)$ and the ratios $f_1^3=\frac{\sigma_{\cdot}}{\sigma_{\cdot}}$; $f_2^3=\frac{\sigma_{\cdot}}{\sigma_{45^\circ}}$; $f_3^3=\frac{\sigma_{\cdot}}{\sigma_{45^\circ}}$ were determined for each moment t of the measurements.

The altitude surveying was carried out by a model for the Venusian atmosphere that was calculated from the results of temperature and pressure measurements, simultaneously carried out aboard Venera-9 and Venera-10, using the equations for hydrostatic equilibrium and quasi-regular descent of the capsule by parachute and aerodynamic flap. The procedure for such calculations is similar to that considered in [5]. The resulting

altitude profiles for T and p are close to previously calculated model distributions [7]. In the segment 61-49 km, the average rate of descent was V = 10-15 m/sec. The time for the measurements by the nephelometers during the descent in the atmosphere of Venus was 50 minutes aboard Venera-9 and 47 minutes aboard Venera-10. /32

From the initial field of experimental points, average curves for the altitude dependences $f^{e}_{1,2,3}(h)$ were obtained, the appearance being shown in Figure 18. The root-mean-square deviation of individual points with respect to the average curves was respectively:

$$\delta_{f_1} = 5\text{-}7\%; \quad \delta_{f_2} = 10\text{-}15\%; \quad \delta_{f_3} = 15\text{-}20\%.$$

The functions $f^{e}_{1,2,3}(h)$ enable the estimation of the aerosol characteristics μ, n, and r_e with respect to altitude and enable the determination of the scattering coefficient $\sigma(h)$, the optical thickness $\tau(h)$, and the concentration of particles $N(h)$ from the altitude profiles $\overline{\sigma}_{\theta_j}(h)$ in accordance with relations (16, 17, 18).

For practically each of the aerosol models having definite values of μ, n, and $\varkappa$, r_e values, corresponding to the experimental values for the functions $f^{e}_{1,2,3}(h)$, were found by the nomograms that reflect the correlation of the functions $f_{1,2,3}$ with the parameters μ, n, $\varkappa$, and r_e. The results of such a selection are represented graphically in the form of dependences $r^{1,2,3}_{e}(h)$ which, in the general case, do not concur with each other. The mutual disposition of these curves varied in dependence on the parameters of the particular models. This indicates that, in various cloud layers, not only the effective particle size r_e, but also other microphysical characteristics of the aerosol vary with altitude. A criterion for the choice of aerosol models at a given height h is the coincidence of

γ_e values that have been determined by experimental values with an accuracy to the measurement error. /3

The measurement results of the Venera-9 were used to obtain data as to $\sigma_{\theta_i}(h)$ through all the measurement channels from 62 to 32 km. The greatest intensities of the signals in all the measurement channels were registered in the altitude region from the beginning of the measurements, i.e. $\sim$62 km, to $\sim$49 km, which should apparently be attributed to the greatest turbidity of the medium, associated with the situation of the main cloud layer here. Below 49 km, the function $\sigma_{4^\circ}(h)$ is reduced to zero; $\sigma_{15^\circ}(h)$ is close to the limit of sensitivity of the channels, while the function $\sigma_{45^\circ}(h)$ retains rather large values, somewhat increasing as the altitude diminishes to $h \simeq 32$ km, where the small-angle nephelometer unit was switched off. The function $\sigma_{180^\circ}(h)$ increases 2-3 times in the range h = 50-40 km from minimum values (nonetheless considerably surpassing the limits of sensitivity of the channels), attains a maximum at $h \simeq 20$ km, and thereafter declines gradually down to $h \simeq 14$ km. At this height, the measurements of the reverse-scattering nephelometer units were terminated. Correspondingly, at $h \lesssim 49$ km, the estimates have a more approximate nature than for the higher regions of the atmosphere, but the relative change in the scattering characteristics of aerosol formations and their vertical structure can be described with sufficient accuracy.

The measurement results of the Venera-10 give information that is similar in quality to the measurements of Venera-9, the only difference being that the small-angle nephelometer was turned off somewhat earlier, at $h \simeq 44$ km, while the reverse-scattering nephelometer was apparently subjected, in the segment $h \gtrsim 50$ km, to the action of strong electromagnetic interference, distorting the results obtained in this segment. Upon further descent in the atmosphere below the above-mentioned height, the functioning of this unit was fully restored and the behavior of the fuction $\sigma_{180^\circ}(h)$ is entirely similar to the measurement data aboard the

Venera-9.

8. The Characteristics of the Aersol Component According to the Measurement Results of Venera-9.

/34

Figures 19 and 20 show the families of curves $\gamma_e^{1,2,3}(h)$, found from the values $f_{1,2,3}^e(h)$ by comparing them with the functions $f_{1,2,3}$ for various aerosol models. By analyzing the nature of the dependences of $\gamma_e(h)$ at variations for μ, n, and $\mathcal{H}$, it is possible to conclude that the properties of the aerosols in the Venusian atmosphere change by layers in accordance with the altitude course of the functions $\overline{\sigma}_{\theta_j}$, which reflect the laminar structure of the clouds (cf. Fig. 22). In the basic cloud layer between 62 and 49 km, it is possible to separate the following regions: The upper layer 61.5-57.5 km (I), a transitional region 58-57 km (I'), a lower layer 57.5-51 km (II), a transitional region 52-51 km (II'), and the zone for the lower limit of the clouds 51-49.5 km (III).

For the upper layer I, as the refractive index changes from 1.5 to 1.4, the values of $\gamma_e^1(h)$ and $\gamma_e^2(h)$ initially coincide or are rather close to each other but noticeably diverge when $n \lesssim 1.45$. The values of $\gamma_e^3(h)$ are less than $\gamma_e^1(h)$ and $\gamma_e^2(h)$ at $n \gtrsim 1.5$; at $n \simeq 1.46$-1.47, these values are rather close to each other and at $n \lesssim 1.45$, $\gamma_e^3(h)$ becomes considerably greater than γ_e^1 and $\gamma_e^2(h)$. As the parameter for the width of the distribution varies from μ = 8-20 to μ = 1-2, the divergence in $\gamma_e^{1,2,3}(h)$ values rises.

Proceeding from the results of the selection of dependences $\gamma_e^{1,2,3}(h)$ at variations of the parameters μ and n and with an allowance for the measurement error, it is possible to assume the following model of the aerosol component for region I:

- The effective particle size of the aerosol increases monotonically from 1.0 ± 0.05 to 1.35 ± 0.1 μm as the height h above the planet surface changes from 61.5 to

58 km.

- the refractive index for the substance of the aerosol particles is

$$n = 1.46 \pm 0.01 \quad (\lambda = 0.92);$$

the size distribution of particles is relatively narrow and the most probable value for the width parameter $\mu = 12^{+8}_{-4}$. Accordingly, the modal size is from $r_0 = 0.8 \pm 0.1$ μm to $r_0 = 1.1 \pm 0.15$ μm. /35

The transitional region (I') is characterized by two features. Upon further synchronous rise in $r_e'(h)$ and $r_e^2(h)$, a certain discrepancy is detected in their values which is not removed upon variations of the parameters μ and n and which exceeds the limit of measurement error. It is possible that this is explained by a certain deviation of the particle distribution from a supermode Gamma-distribution. Considering that $r_e'(h) > r_e^2(h)$ in this case, from qualitative considerations it is possible to suppose the appearance of a more coarse-dispersed fraction of particles in the base of the upper layer. This assumption is entirely tangible if it is considered that the lower layer of clouds consists, as we see, of more coarse particles. Furthermore, the dependence of $r_e^3(h)$ at $n \simeq 1.46$-1.47 becomes noticeably diminishing with a reduction in altitude. The variation of the parameter n toward a gradual diminishing to 1.42-1.40 conducts $r_e^3(h)$ to values that are close to $r_e'(h)$ and $r_e^2(h)$. The refractive index for the substance of the particles changes from $n = 1.46^{+0.02}_{-0.01}$ to $n = 1.42 \pm 0.015$, the effective particle size r_e increases from 1.35 ± 0.10 μm to $1,60 \pm 0.10$ μm. This enables the supposition that in the transitional layer (I') there occur definite changes not only in the microstructure but also in the properties of the aerosols, most likely associated with a change

in temperature but possibly also with a change in the nature of particles.

In the lower layer II there occurs a gradual increase in the particle sizes from 1.6 ± 0.1 μm to 1.9 ± 0.2 μm. In this case the curves $z_e^1(h)$ and $z_e^2(h)$ are close, while the variations of n and μ do not exert a considerable influence on their mutual disposition. However, when $n > 1.42$ and the distribution is widened to μ = 1÷2, $z_e^3(h)$ is considerably removed from the values for $z_e^1(h)$ and $z_e^2(h)$. In the lower portion of this layer, /36 estimates for the parameter n become less determinate since, as already observed earlier, when 1.7 μm $\lesssim z_e \lesssim$ 2.4 μm and when $n \simeq$ 1.33-1.5, the function $f_3(n, \mu, z_e)$ is poorly and ambiguously dependent on Nonetheless, in this portion of the cloud a tendency to the reduction of n can be traced. The value of the lower limit is here permitted to attain n 1.33, although the reliability of the estimate for this magnitude is not high. It should however be remarked that the presence of a certain absorption in this portion of the layer in limits to $\varkappa$ values $\simeq 3 \cdot 10^{-3}$ renders the coincidence of $z^{1,2,3}(h)$ also sufficiently complete for n = 1.42 ± 0.015. In this region the preferred value for the parameter of the distribution width is $\mu = 12_{-4}^{+8}$.

The transitional region (II'), is characterized by the fact that the effective particle sizes of the aerosol diminish to $z_e \simeq 1.5$ μm and then increase to $z_e \simeq$ 1.6-1.7 μm in the lower portion of the region. Near the base of the lower layer, the particle sizes again diminish. Further, judging by the nature of the behavior for $z_e^{1,2,3}$ with respect to each other, there occurs a certain rearrangement of the aerosol structure.

Estimates for the refractive index give values of n = 1.42 ± 0.01, while the preferred value for the width parameter becomes μ = 2 ÷ 4.

The region (III) may be called the zone of the lower cloud

limit, in which the values of all the measured indices for the directional light scattering $\sigma_{\theta_j}(h)$ fluctuate synchronously in a broad range of values and in the lowermost portion of the zone diminish to minima. The effective particle size also fluctuates and is r_e = 1.5-1.6 μm in the optically more dense segments and $r_e \simeq$ 1.3-0.9 μm in the less dense segments. Judging by the nature of the altitude course of $r_e^{1,2,3}(h)$, for variations of r_e, the index of refractions has here values in the limits n = 1.40-1.43. The appearance of the obtained characteristics $r_e(h)$ and $\nu(h)$ at μ = 8-20 is shown in Figure 21.

Using the obtained laminar-microphysical models of the aerosols in conjunction with data from measurements of the absolute values of $\sigma_{\theta_j}(h)$, it is possible to determine a number of integral optical and physical characteristics of the cloud layer. /37

Considering that $\bar{\sigma}(\theta_j) = \sigma \cdot i(\theta_j)$, we shall determine the coefficient of scattering $\sigma(h)$. For the calculations we shall use the results of measurements of $\sigma_{45^\circ}(h)$ and calculated values for $\bar{i}(45^\circ)$, in accordance with the values of the parameters $r_e(h)$, $\mu(h)$, and $n(h)$ from the obtained aerosol models. The altitude profile of the space coefficient of scattering $\sigma(h)$ is shown in Figure 22.

Obviously, the two basic layers I and II are most characteristic for the clouds of Venus along the route of descent of the Venera-9 descent capsule. In these layers, for wave lengths λ = 0.92 μm of the radiation, the coefficient of scattering is, respectively, $\sigma_I = (2+3)\cdot 10^{-5}$ cm^{-1} and $\sigma_{II} = (3+5)\cdot 10^{-5}$ cm^{-1}. In layer III (lower limit), the values of σ_{III} fluctuate in limits of $(0.3+2)\cdot 10^{-5}$ cm^{-1}.

Using the obtained estimates for the characteristics of the Venusian clouds and calculations for the average factor of scattering effectiveness, partially presented in Table 4, for a wave length of λ = 0.55 μm the index of scattering is σ_I = (1.75 + 2.6)$\cdot 10^{-5}$ cm^{-1} and σ_{II} = (2.75+4.6)$\cdot 10^{-5}$ cm^{-1}, which corresponds to a meteorological range of visibility S_{vis} = (1.7+1.15) km and

(1.1+0.65) km for a threshold of contrast sensitivity ε = 5%. The optical thickness of the clouds was computed with the help of relation (17). The appearance of the curve $\tau(h)$ is shown in Figure 22. The optical thickness of the upper layer I is approximately τ_I = 7, of the lower layer τ_{II} = 26, of the layer for the lower boundary of the cloud $\tau_{III} \simeq 2$, and of the entire cloud layer $\tau \simeq 35$.

The altitude dependence for the concentration of aerosol particles N(h), calculated in accordance with (18), is shown in Figure 22. The concentration of particles in layer I is N = 200-350 cm^{-3}, in layer II N = 250-300 cm^{-3}, and in the region of the lower cloud boundary, N = 50-150 cm^{-3}. /38

The results obtained below 49 km, i.e. in the atmospheric layer under the clouds, are of special interest. As already remarked, when $h \lesssim 49$ km the values of the indices for the directional scattering $\sigma(\theta_j)$ are sharply reduced. In this case the values of $\sigma_{4°}(h)$ are beyond the limits of sensitivity of the channels and are $\sigma_{4°}(h) <$ or $\ll 10^{-3}$ steradians^{-1}m^{-1}; $\sigma_{15°}(h)$ is at the limit of sensitivity of the channels and is not more than $2 \cdot 10^{-4}$ steradians^{-1} m^{-1}, while the value of $\sigma_{45°}(h)$ gradually rises from $0.2 \cdot 10^{-4}$ steradians^{-1}m^{-1} at a height h = 46 km to $2 \cdot 10^{-4}$ steradians^{-1}m^{-1} at a height h = 32 km, where the small-angle nephelometer was switched off. The results of the measurements in the 180° channel were obtained in the most complete volume, while the values of $\sigma_{180°}(h)$ considerably exceed the limits of sensitivity of the channel. The values of $\sigma_{180°}(h)$ also rise gradually from $(2+3) \cdot 10^{-5}$ steradians^{-1}m^{-1} at h≃46 km to $(13-14) \cdot 10^{-5}$ steradians^{-1}m^{-1} at h = 18-20 km, and then dropped to $(3+5) \cdot 10^{-5}$ steradians^{-1}m^{-1} at h = 14 km, where the measurements by the reverse-scattering nephelometer were concluded. The values of $f^e_{1,2,3}(h)$ in this case can only be established in the form of inequalities: $f^e_1(h) <$ or $\ll 5$; $f^e_2(h) < 5$. The value of $f^e_3(h)$ gradually diminishes from 0.4-0.6 at a height of 40-45 km to 0.2-0.3 at a height of

33-32 km. comparing the obtained experimental data of $f^{e}_{1,2,3}(h)$ with theoretical calculations for $f_{1,2,3}(\rho_э, \mu, n, \varkappa)$, it is possible to establish with complete determinacy that the atmosphere beneath the clouds contains a very finely dispersed aerosol with dimension in the limits of $\rho_e \simeq 0.08\text{-}0.16\ \mu m$. However, it is difficult to obtain here an estimate for the index of refraction, due to the slight sensitivity of the obtained values of functions $f_{I,2,3}(\tau_э, n, \mu, \varkappa)$ to the change in the parameter n and due to the insufficient volume of experimental data. The indicatrix of scattering for such aerosols, for scattering angles close to $\theta \simeq 45°$, is equal to $\bar{\tau}_{45} = 0.15\text{+}0.22$ steradians^{-1}. From this we obtain an estimate for the index of scattering $\sigma(h)$, which is $\sigma \simeq 0.3 \cdot 10^{-5}$ cm^{-1} at altitudes h = 40+45 km and $\sigma \simeq 0.6\text{-}0.9 \cdot 10^{-5}$ cm^{-1} at altitudes h = 32-40 km. The optical thickness of the 49-32 km layer in this case turns out to be τ = 7-8. /39
Further, there may be located here large particles with $\rho_e \gg 2\ \mu m$ (bimodal distribution), with a high index of refraction ($1.7 < n < 2.0$ at $N \lesssim 2$ cm^{-3}) in accordance with [8]. In the 32-14 km region, these particles apparently make a certain contribution to the scattering, although the atmosphere is rather transparent here (at $N \lesssim 6$). The magnitude of τ is estimated in the limits of 3-5.

9. Characteristics of the Aerosol Component According to the Venera-10 Measurement Results.

According to the measurement results in the region of descent of Venera-10, reliable data were obtained as to $\sigma_{\mu°}(h)$, $\sigma_{15°}(h)$, and $\sigma_{45°}(h)$ in the interval of altitudes 61-44 km and as to $\sigma_{180°}(h)$ in the interval 48-17 km. The general nature of the dependences $\sigma_{\theta_3}(h)$ is in good agreement with the measurement results of Venera-9. Three basic cloud layers are also traced, corresponding to the altitude interval 61-58 km (I), 58-51 km (II), and 51-48 km (III), the lower boundary of the clouds being much more sharply indicated in the Venera-10 region of descent. The lower layer of clouds III, compared to the region of Venera-9, is optically more homogeneous here, while the lower boundary of clouds lies somewhat lower.

The data of $\sigma_{180^\circ}(h)$ testify to the fact that the aerosol beneath the clouds has practically the same nature of altitude distribution, although in the altitude intervals 47-42 km and 38-28 km, $\sigma_{180^\circ}(h)_{V-10} > \sigma_{180^\circ}(h)_{V-9}$ by 1.5-2 times, which may be due to either a greater concentration of particles or to a somewhat different microstructure of the aerosol and its size distribution.

Estimates for the effective particle size z_e are also carried out by means of $f_1^e(h)$ and $f_2^e(h)$. Since there is an absence of data as to $\sigma_{180^\circ}(h)$, and correspondingly as to $f_3^e(h)$ for the base cloud layer, and since the variations of the parameters n, $\mathcal{H}$, and μ have an insignificant influence on the results of the estimates, the nature of the dependences $n(h)$ and $\mu(h)$ was assumed to correspond to that obtained by the measurement data of Venera-9. The effective particle sizes in the upper cloud layer rises from $z_e = 1.1 \pm 0.1\,\mu m$ to $z_e = 1.3 \pm 0.15\,\mu m$. In /40
the region of trasition from the upper to the lower layer, the effective particle sizes also rise, although the estimates for z_e by $f_1^e(h)$ and $f_2^e(h)$ gradually diverge, as for the data of Venera-9, but with the difference that this divergence continues for the entire lower layer and comprises $\bar{r}_3(h) \pm 15\%$ with respect to the average curve. This passes beyond the limits of the measurement errors and can be explained by a deviation of the actual size distribution of the particles from the unimodal Gamma-distribution. Numerical experiments show that a bimodal law for the size distribution of the particles with effective sizes of $z_e \lesssim 0.3\,\mu m$ for the fine fraction and $z_e \simeq 2\text{-}3\,\mu m$ for the coarse fraction can be assumed as one of the possible variants in the lower cloud layer.

10. Evaluation of the Results

The characteristics of the aerosol component of the Venusian atmosphere, obtained from an analysis of light scattering data, are summarized in Table 5 and in Figures 22 and 23, where they are shown in dependence on the altitude with simultaneously adduced

temperature and pressure curves in accordance with the model [7]. The entirety of these characteristics determines the microphysical properties of the aerosol and the structure of the Venusian clouds with an allowance for the mentioned measurement errors and the assumed procedure for interpreting the experimental data. The analysis made use of a broad class of calculation models, giving the dependences of the directional scattering coefficients on the determining parameters of the aerosol. On the basis of these results a number of considerations may be expressed in regard to the peculiarities of the clouds.

I. The main cloud layer, in the form of a thin fog or mist, is comprised of polydispersed particles of almost uniform composition that do not differ greatly as to size. The clouds /41 are stable and do not have sharply pronounced spatial inhomogeneities; the structure and microphyiscal properties differ insignificantly at a distance of $\sim$2,000 km along the horizontal.

In the daytime, the lower boundary of the clouds is located at an altitude of 49 km above the surface, according to Venera-9, and 48 km according to Venera-10. This discrepancy can be explained by the different zenith angles of the Sun at the descent sites (33° for Venera-9 and 27° for Venera-10), if we consider the inertial delay in the atmosphere heating at altitudes of $h \geqslant 30$ km, where the daily variation in temperature beings to appear.

In the cloud region it is possible to distinguish three superjacent zones (layers) with different microphysical and optical characteristics (cf. Tab. 5), so that the Venusian clouds cannot be regarded as being uniformly mixed or, consequently, entirely homogeneous. The layers, however, are not isolated from each other and their properties are mutually interconnected.

TABLE 5

/42

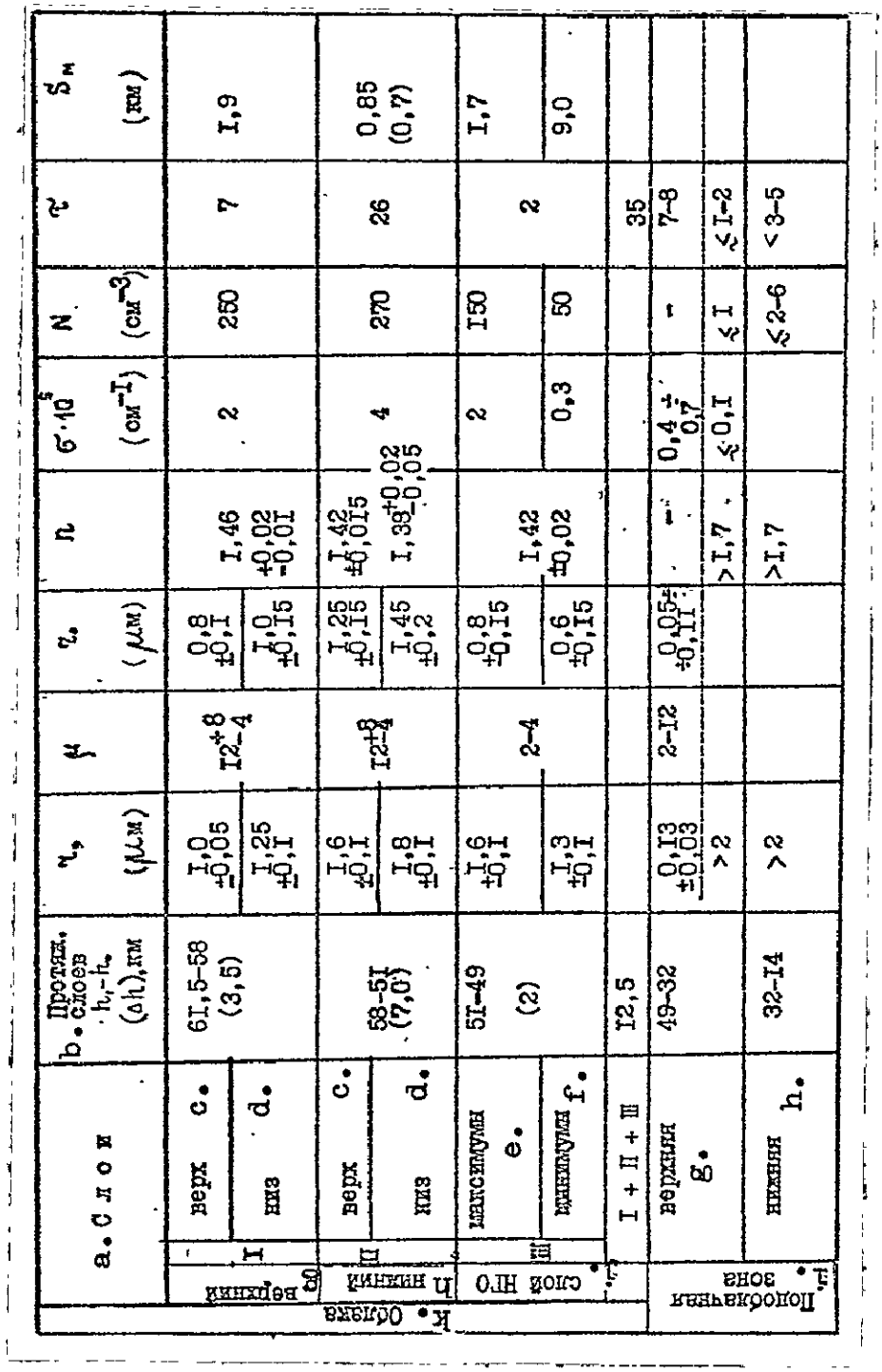

k. Отдача	a. Слои	b. Протяж. слоев h_1-h_2 (Δh), км	r_1 (μм)	μ	r_0 (μм)	n	$\sigma \cdot 10^5$ ($см^{-1}$)	N ($см^{-3}$)	τ	$\delta_м$ (км)
верхний I	верх c.	61,5-58 (3,5)	1,0 ±0,05	12-8 4	0,8 ±0,1	1,46 +0,02 -0,01	2	250	7	1,9
	низ d.		1,25 ±0,1		1,0 ±0,15					
нижний II	верх c.	58-51 (7,0)	1,6 ±0,1	12-8 4	1,25 ±0,15	1,42 ±0,015	4	270	26	0,85 (0,7)
	низ d.		1,8 ±0,1		1,45 ±0,2	1,38 +0,02 -0,05				
слой НПО III	максимумы e.	51-49 (2)	1,6 ±0,1	2-4	0,8 ±0,15	1,42 ±0,02	2	150	2	1,7
	минимумы f.		1,3 ±0,1		0,6 ±0,15		0,3	50		9,0
I + II + III		12,5							35	
Подоблачная зона верхняя	g.	49-32	0,13 ±0,03	2-12	0,05 ±0,11	-	0,4 ÷ 0,7	-	7-8	
			>2			>1,7	≤0,1	≤1	≤1-2	
нижняя	h.	32-14	>2			>1,7		≤2-6	> 3-5	

Key: a, layers; b, extent of the layers; c, top; d, bottom; e, maximum; f, minimum; g, (over)

Key to Table 5 (Cont.): g, upper; h, lower; i, sub-cloud zone; j, layer of lower cloud limit; k, clouds. (Note: commas in tabulated material equivalent to decimals).

2. The obtained estimates show that the spectrum of cloud particles is represented by a curve with a single peak, for example, a Gamma-distribution, with effective size 2_e from 1.0 to 1.35 μm in the upper layer, from 1.6 to 1.9 μm in the lower layer, and with the width parameter of the distribution within the bounds 8-20. However, in the region of transition from layer I to layer II, indications have been found that the spectrum of particle size differs from the unimodal distribution. It can be assumed that there exists here in a variable (depending on the altitude) ratio two fractions of particles, not only with different 2_e but, possibly, also different indices of refractions.

3. As a consequence of the low optical density, corresponding to values of $\sigma = (2\text{-}4)\cdot 10^{-5}$ см$^{-1}$, the meteorological range of visibility along the entire thickness of the clouds is high, being not less than 0.7-0.8 km. At an average concentration of $N \simeq 250$ cm^{-3}, /43 the distance between the cloud particles is ~1.5 mm. The small concentrations and sizes of the particles are responsible for the slight mass of the cloud condensate. Its absolute volume content q for each of the above layers and the mass proportions of the mixture $\rho_{PR.}$ (for a condensate density $\bar{\rho}_c \simeq 1.6$g/cm^3) are shown in Figure 22. The average value for the entire cloud does not exceed $\bar{\rho}_{PR.} \simeq 5\cdot 10^{-6}$.

4. The discovered microphysical properties of the clouds in layer I are in good accordance with the values estimated from the results of terrestrial polarimetry observations close to their visible upper boundary (in a layer not more than several hundreds of meters in thickness). The index of refraction, determined from the data of nephelometer measurements, the relatively small

discrepancies in the sizes and concentration of particles throughout almost the entire thickness of the cloud at a considerable change in temperature and pressure with altitude, and also the preservation of a rather narrow size distribution of the particles and the stability of the clouds do not contradict the views that regard the cloud condensate as basically formed from concentrated sulfuric acid [16-17].

5. The nature of the change in microphysical aerosol properties with altitude makes it possible to better understand the nature of the condensate. Proceeding from the sulfuric acid hypothesis and an estimate for the equilibrium vapor pressure of H_2O above the drops, it can be supposed that the mass content of H_2SO_4 and H_2O are comparable in the main cloud stratum. Then, taking into account the molar ratio for the hydrates $H_2SO_4 \times nH_2O$, a relative volume content of $H_2O \gtrsim 3 \cdot 10^{-5}$ below the level of evaporation should correspond to the value $\bar{\rho}_{пр.} \simeq 5 \cdot 10^{-6}$. This lower limit, however, is approximately one order of magnitude less than the value obtained for the lower cloud boundary from the phase diagram for H_2SO_4 and the measurement data of Venera-4 to Venera-6 (cf. [5]). Evidently, taking into account the high efficiency for the solution of H_2SO_4 in water, it should be allowed that the concentration of the solution changes along the thickness of the cloud, to which there corresponds a reduction in the average value of the refractive index from 1.46 to 1.42 and even less in the lower portion of layer II, until conditions are attained for an intensive evaporation of water from the solution near the lower cloud boundary, where n again rises to 1.42. The lowering of n below 1.40 + 1.42 in layer II is possibly associated with the influence of an aqueous solution of HCl, also contained in the drops of the cloud condensate and exerting a perceptible influence on N when the temperature rises. /44

6. The observed small growth in the effective and the modal radius of the particles r_e and r_o with depth signifies that, on the one hand, the individual condensate particles do not attain large sizes and, consequently, the homocoagulation time is

comparable with the mixing time and, on the other hand, a sedementational stability is entirely preserved within the limits of the clouds. Moreover, in the lower layer III there is observed a strong reduction in μ, which may be attributed to the increase in the relative contribution of more coarse particles to the distribution.

7. Below the clouds, the boundary of which probably experiences a certain variation with altitude, an aerosol is present, its characteristics being shown in Table 5. In the region of 49-32 km, they satisfy two models which are not mutually exclusive. The presence of stable signals in the 45° and 180° channels down to a height of 32 km and the absence of signals in the 4° and 15° channels is interpreted as the presence here of a finely-dispersed aerosol ($r_e \sim 0.13\,\mu$m), which is in accordance with the results of an interpretation for measurements of quasi-momochromatic radiation flows from the Sun, simultaneously carried out aboard Venera-9 and Venera-10 [3]. Furthermore, much more coarse particles may be found here, introducing a decisive contribution to the 180° channel by means of the high refractive index ($1.7<\eta\leq 2.0$ at $N\lesssim 2$ cm^{-3}) in accordance with the estimates /45
made by us before [8]. In the region of 32-14 km, where there are only measurements in the 180° channel, these particles apparently contribute the main part to the scattering, but the atmosphere here (at $N\lesssim 6$) is rather transparent. The results of determining the microphysical characteristics of the aerosol below 51 km do not contradict the theoretical model of A. Young [18], according to which sulfur (η = 1.9) plays an important role in the chemism of the Venusian clouds along with H_2SO_4.

Thus, the aerosol throughout the thickness of the Venusian atmosphere, including that detected below the cloud boundary, apparently has a common genetic nature. The correlation of all the characteristics for the aerosol component within the compass of a single model requires a more complete analysis, availing itself of phase diagrams for all the main hypothetical components and compounds, which represents an independent problem. In the

framework of such an analysis it will moreover be possible to substantiate and compare the characteristic times of the basic processes (condensation, coagulation, mixing, photochemistry), ultimately responsible for the formation, the preservation of stability, and other specific features of the Venusian clouds.

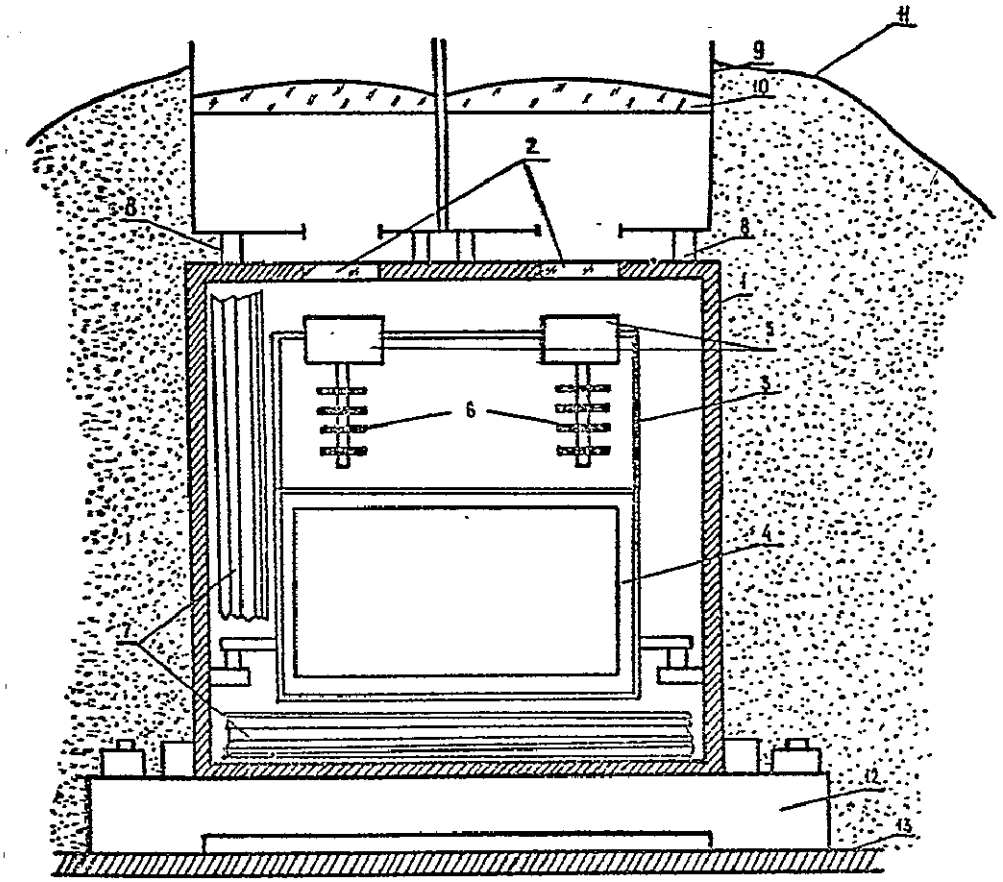

Fig. 1. Heat protection diagram for the instruments of the nephelometer complex (reverse-scattering). 1 - hermetically-sealed housing; 2 - ports; 3 - body of the thermal battery; 4 - compartment for the preliminary amplifier; 5 - photoreceiver and emitter; 6 - radiators; 7 - screening insulation; 8 - heat-insulating collars; 9 - shutters; 10 - lenses; 11 - external heat insulation; 12 - heat-insulating bracket; 13 - body of descent capsule.

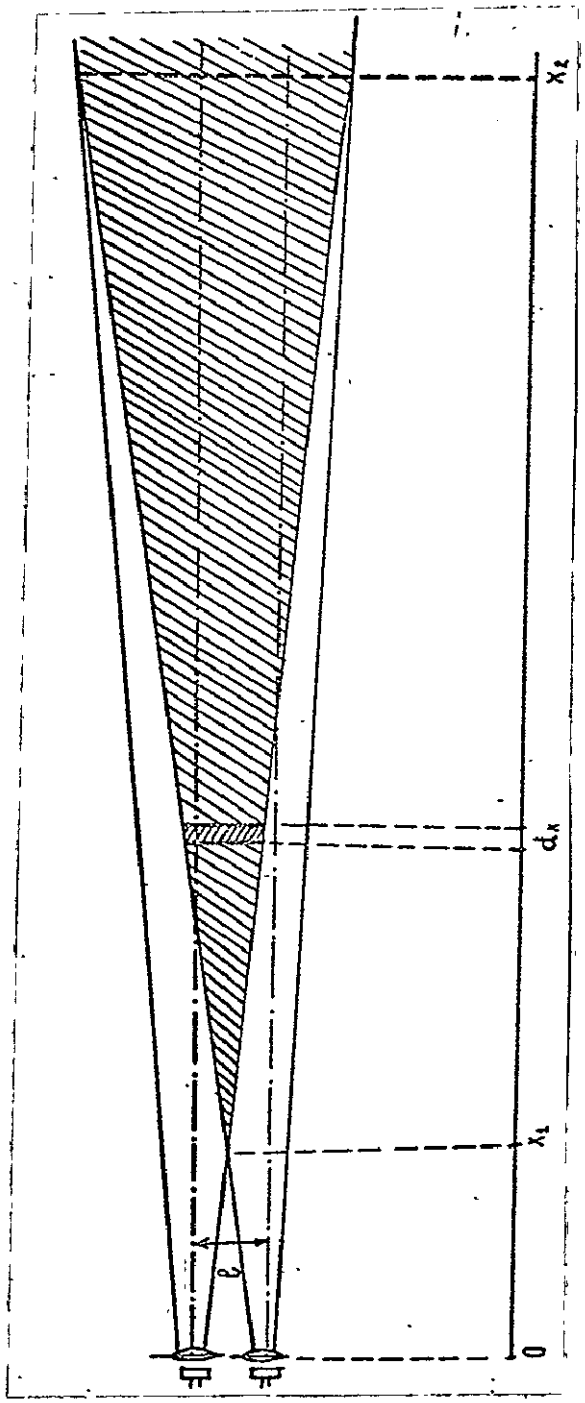

Fig. 2. Specification of the energy characteristics of the reverse-scattering nephelometer.

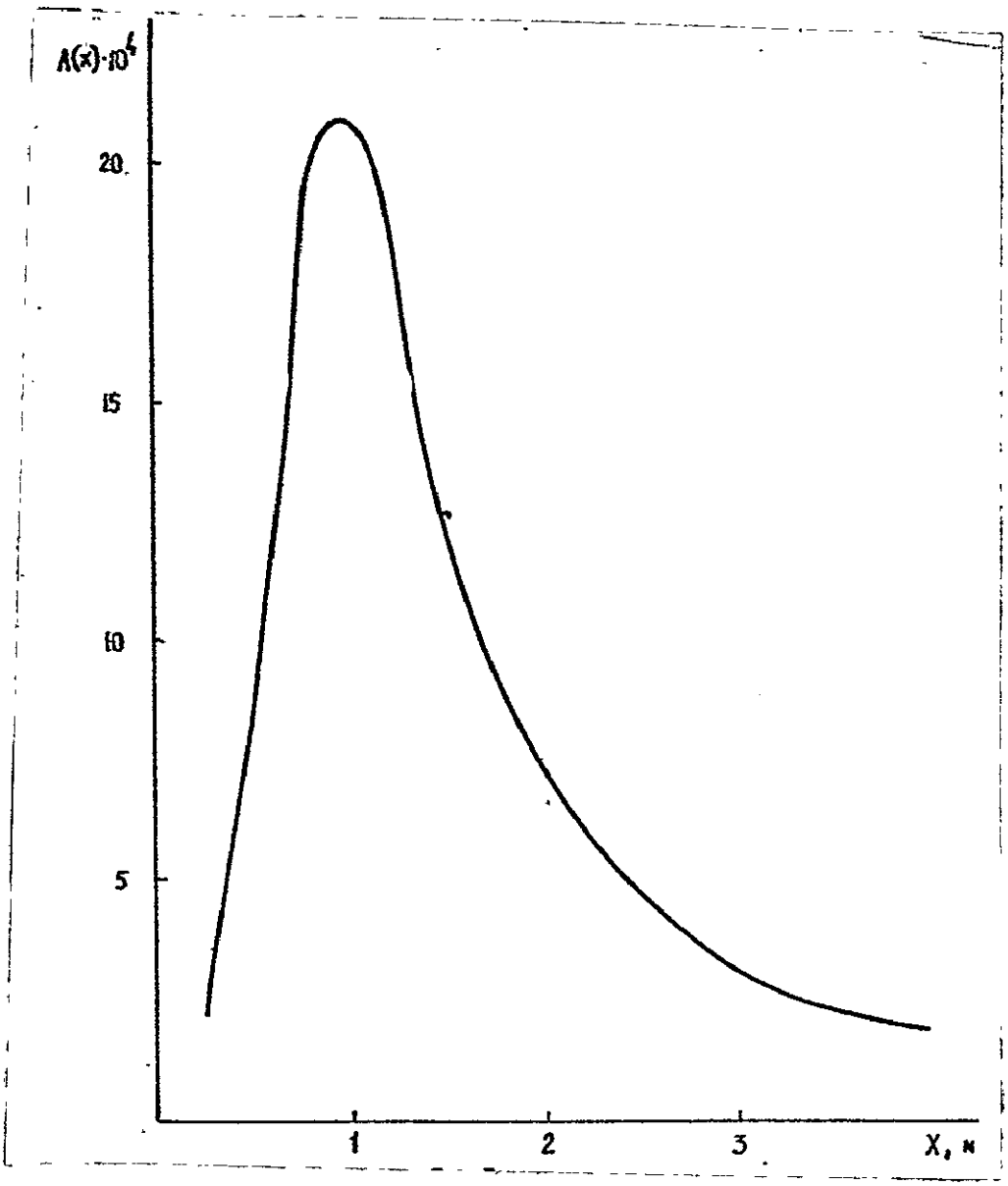

Fig. 3. The function A(X), characterizing the relative contribution of the elements in the scattering volume to the total flux.

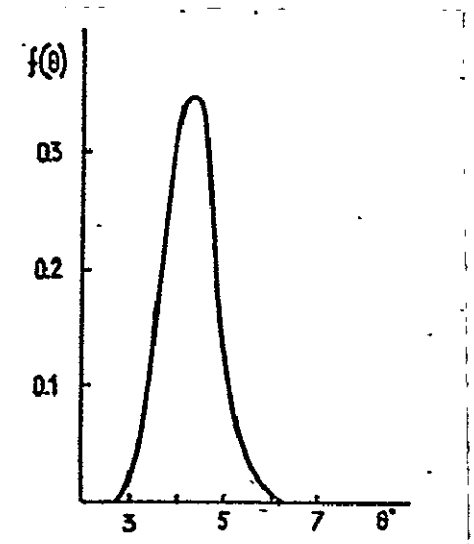

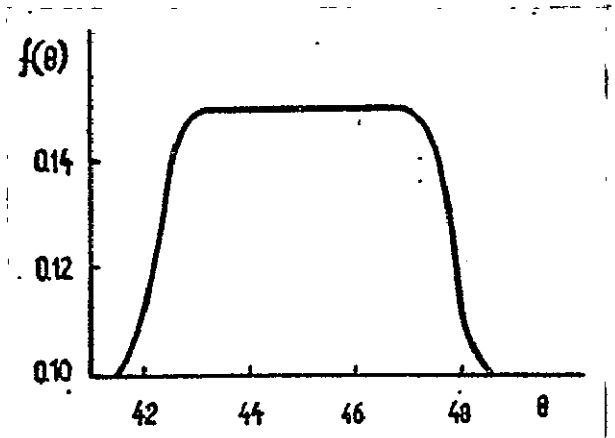

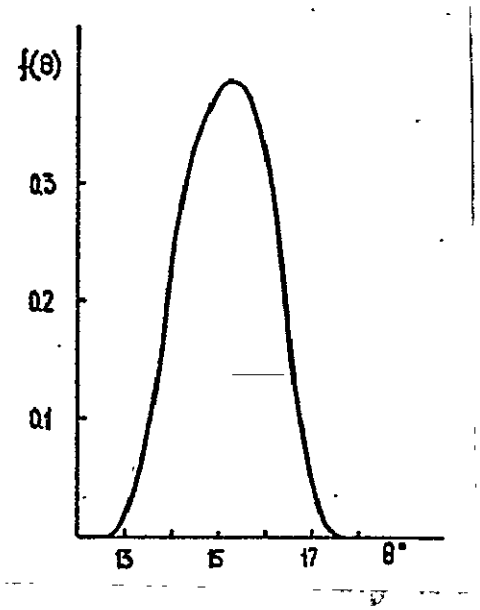

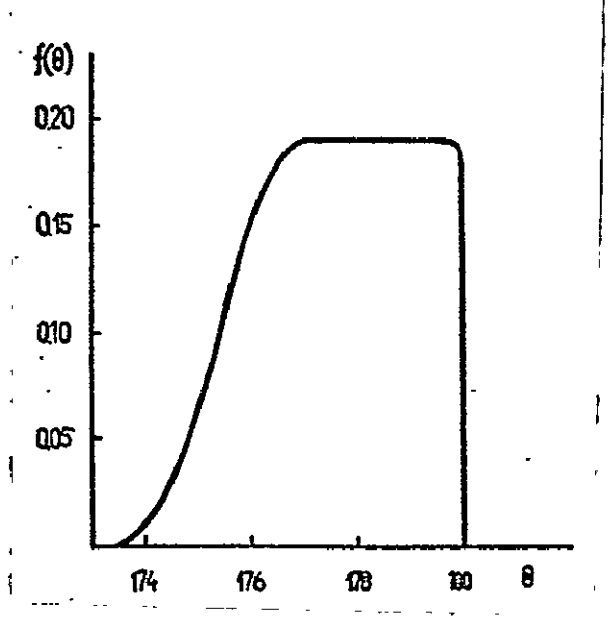

Fig. 4

Fig. 5

The weighting functions of the nephelometer measuring channels.

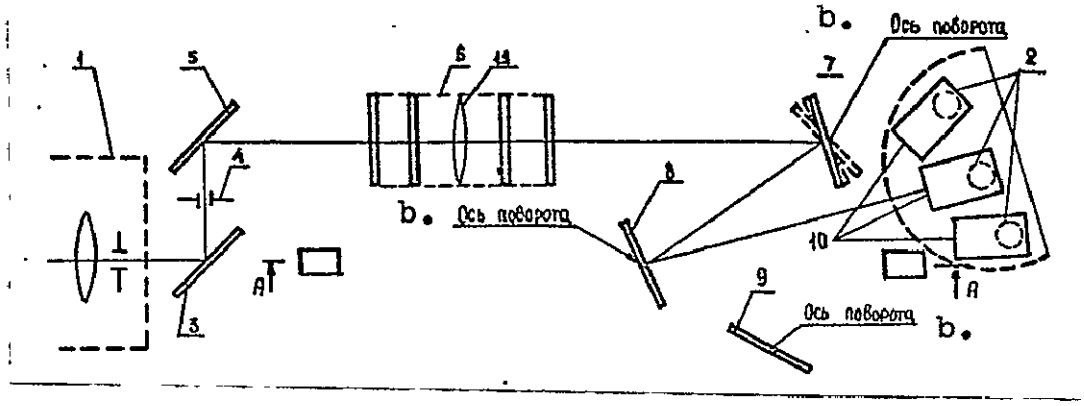

Fig. 6. Optical diagram for the calibration attachment of the low-angle nephelometer: 1 - emitter; 2 - photoreceiver; 3,-5, 7, 8, 9, 10 - mirrors; 4 - diaphragm; 6 - case with attenuators; 11 - lens; Key: b, turning axis.

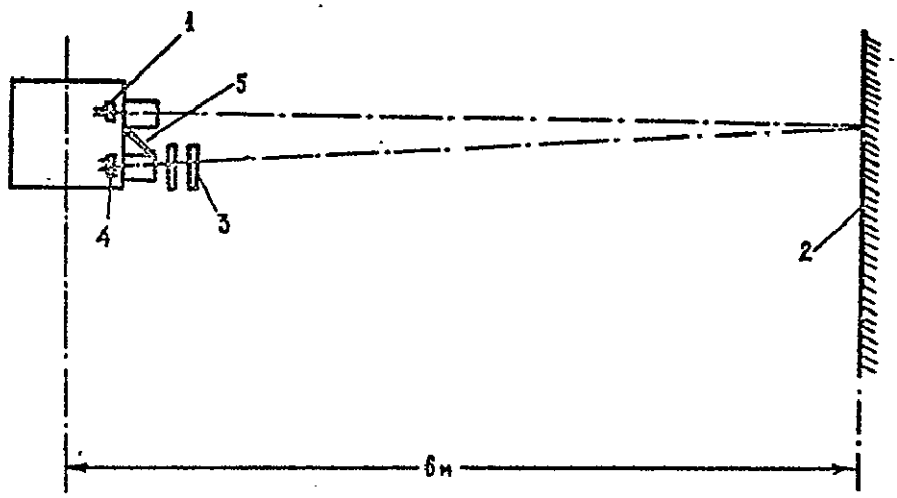

Fig. 7. Optical Diagram for calibration attachment of the reverse-scattering nephelometer: 1 - emitter; 2 - screen; 3 - set of neutral attenuators; 4 - photoreceiver; 5 - reference emission tract.

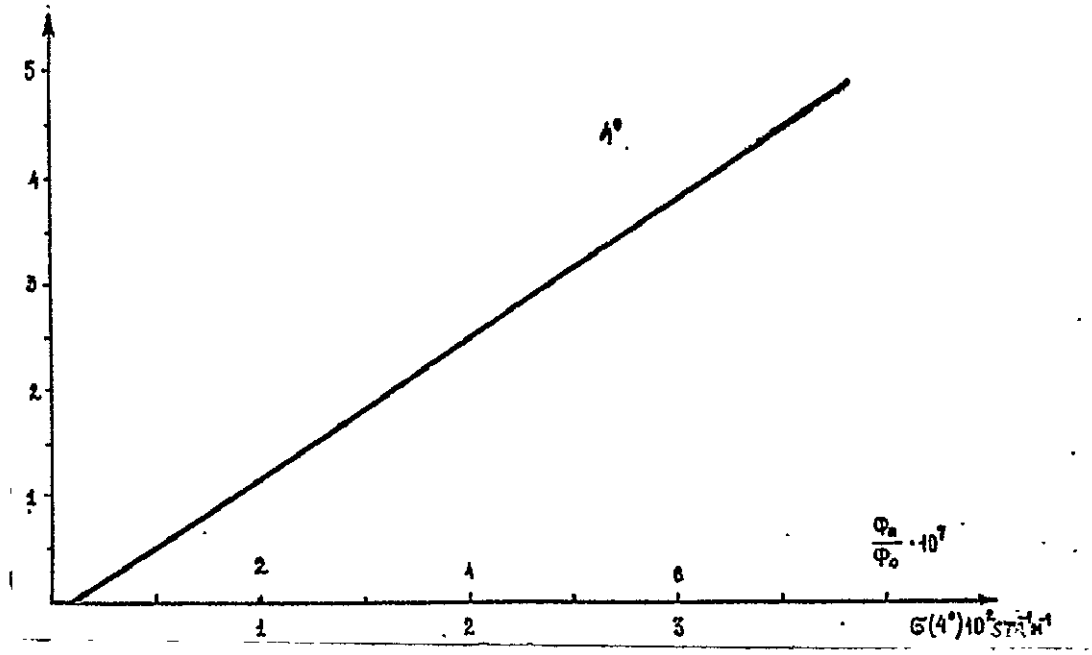

Fig. 8. Calibration characteristic curve for the 4 measuring channel.

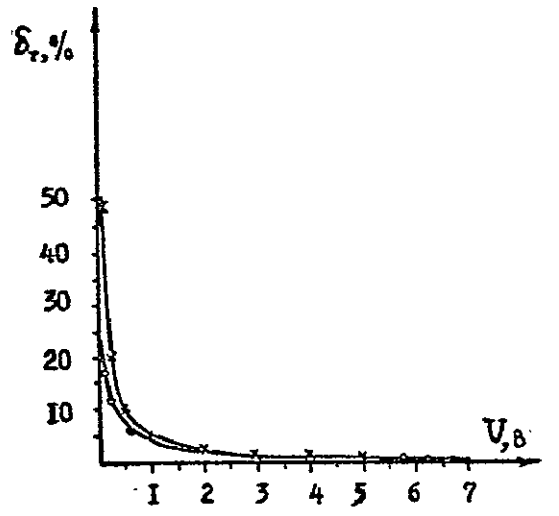

Fig. 9. Dependence of the telemetry errors δ_T (in %) on the magnitude of the output potential U (in Volts).

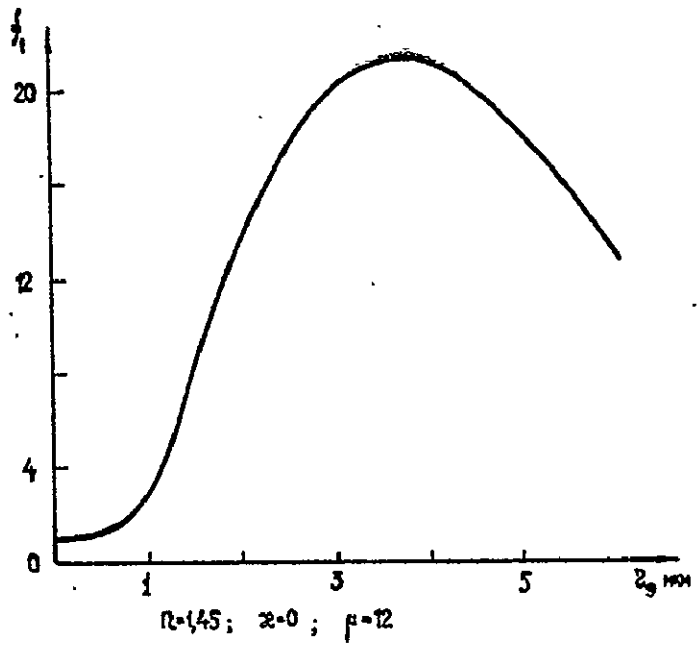

Fig. 10

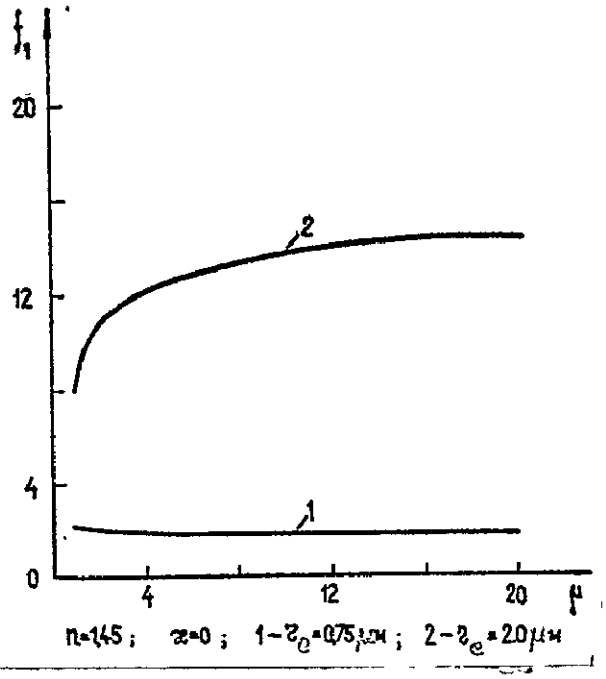

Fig. 11

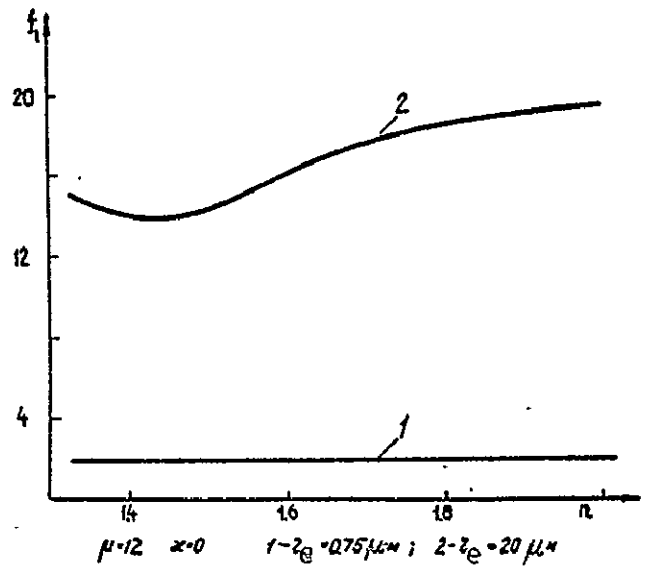

Fig. 12

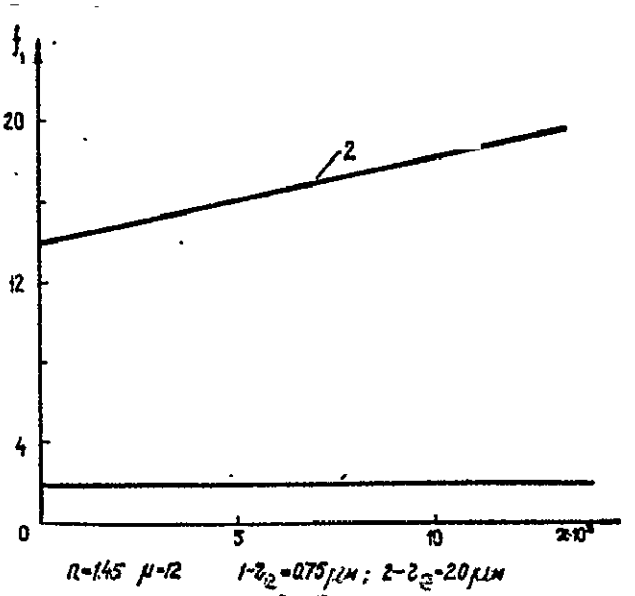

Fig. 13

Figs. 10-17. Dependences of the model functions f_1, f_2, f_3 on the microphysical parameters ℓ_e, μ, n.

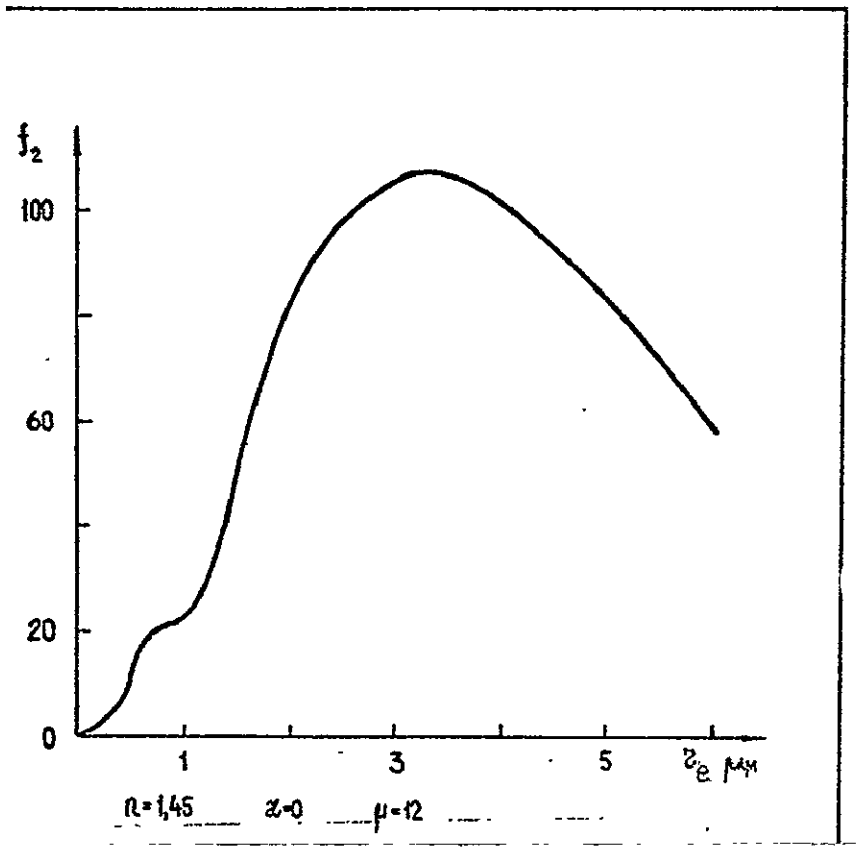
f_2
100
60
20
0
1
3
5
z_e мкм
n=1,45 x=0 μ=12

Fig. 14.

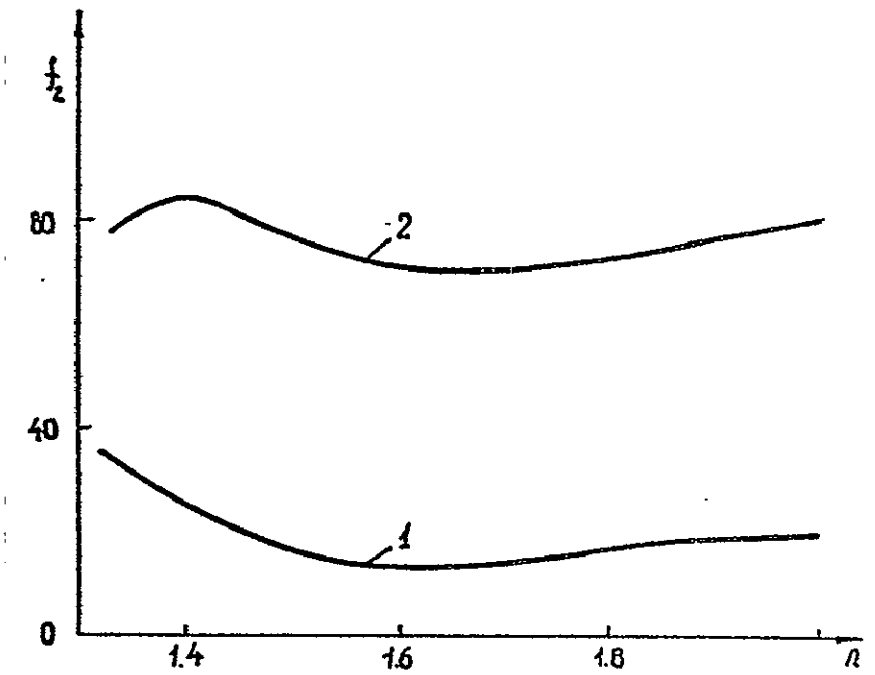
f_2
80
40
0
2
1
1.4
1.6
1.8
n
μ=12 x=0 1-z_e=0.75 мкм 2-z_e=2.0 мкм

Fig. 15.

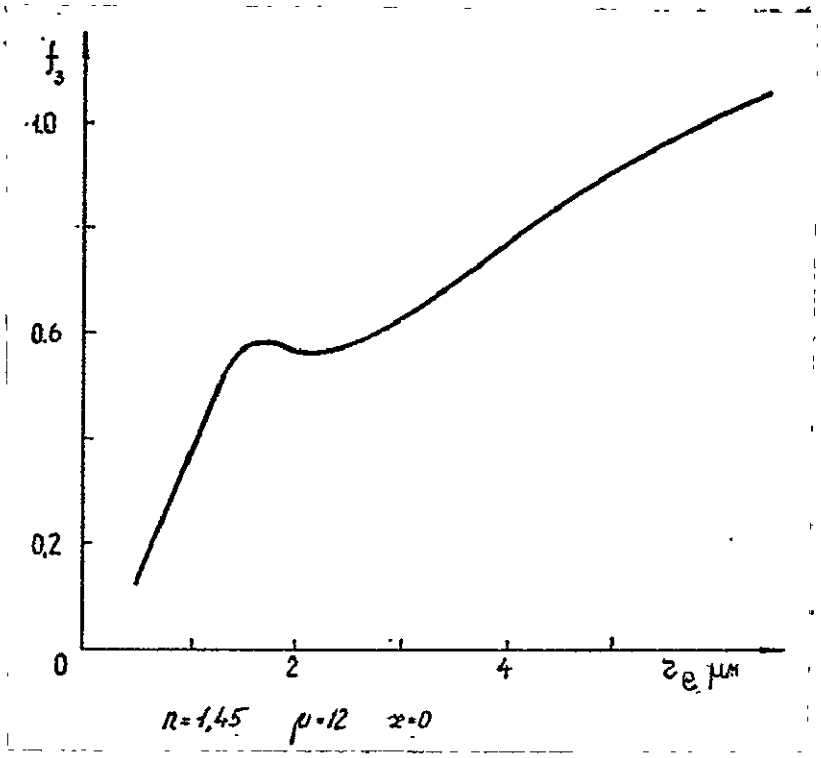
f_3
1.0
0.6
0.2
0
2
4
r_e μм
n=1,45 μ=12 x=0

Fig. 16

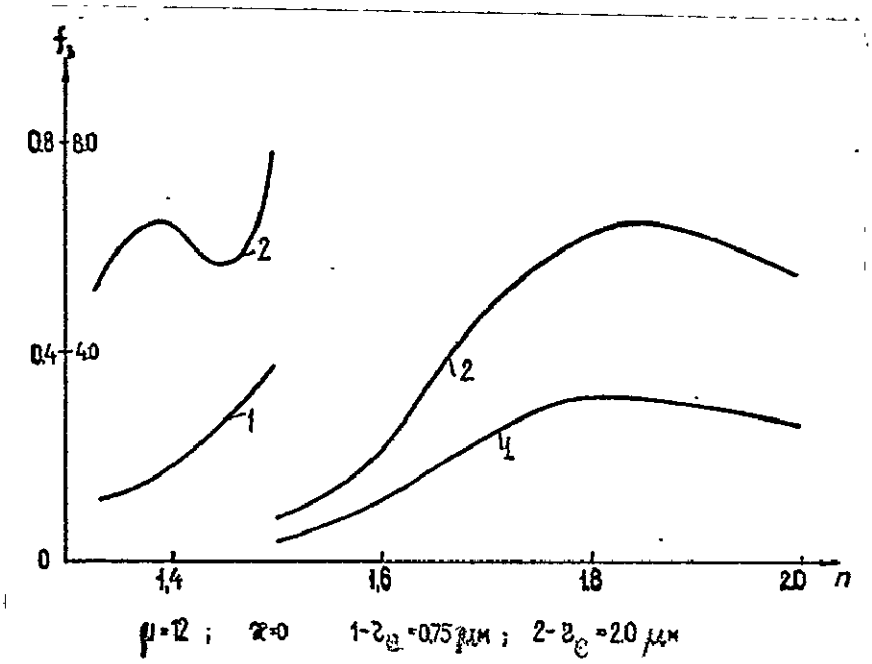
f_3
0.8
0.4
0
8.0
4.0
1,4
1,6
1.8
2.0
n
2
1
2
1
μ=12 ; x=0 1-r_e=0.75 μм ; 2-r_e=2.0 μм

Fig. 17

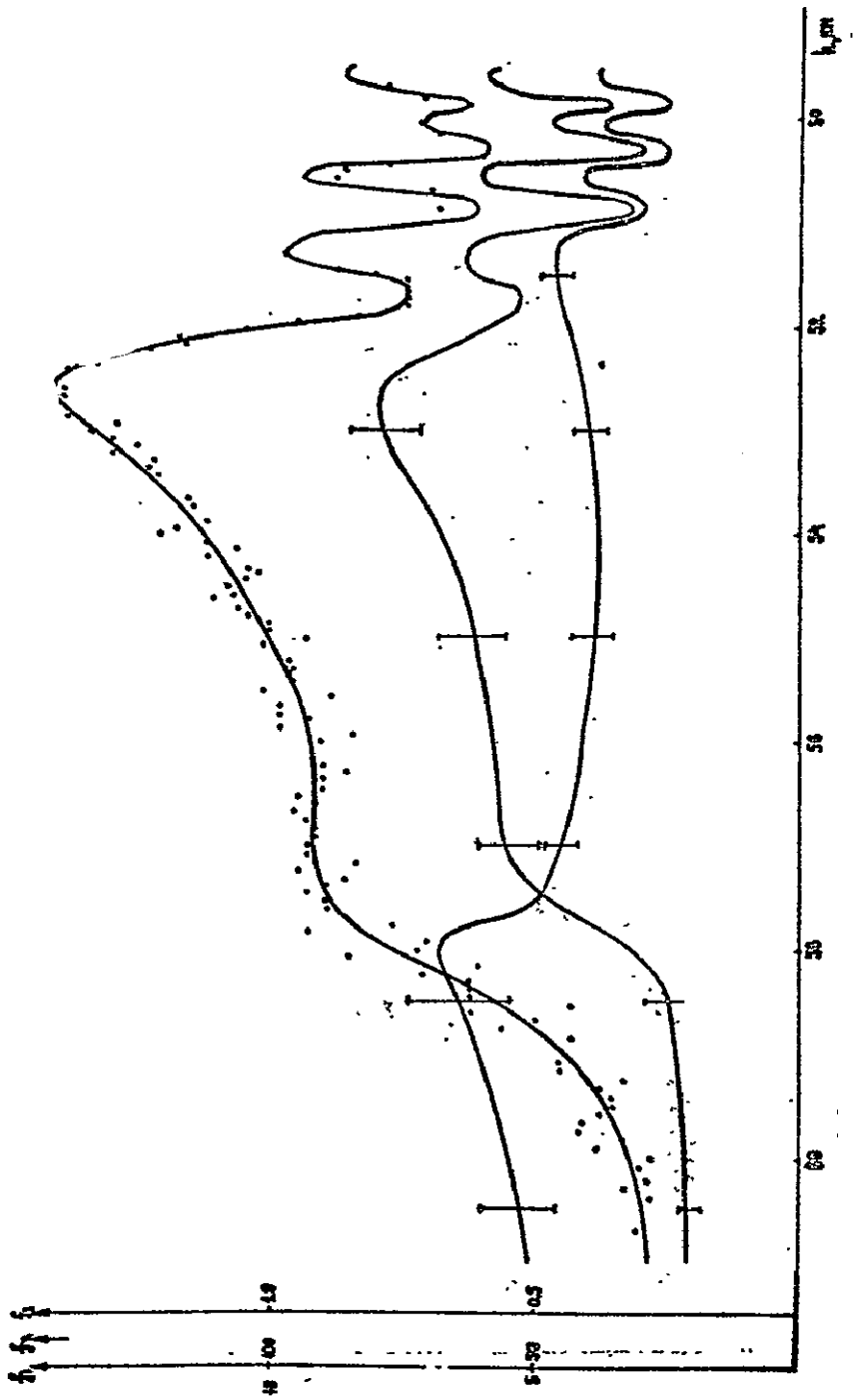

Fig. 18. Dependences of the experimental functions f_1^e, f_2^e, f_3^e on the height h.

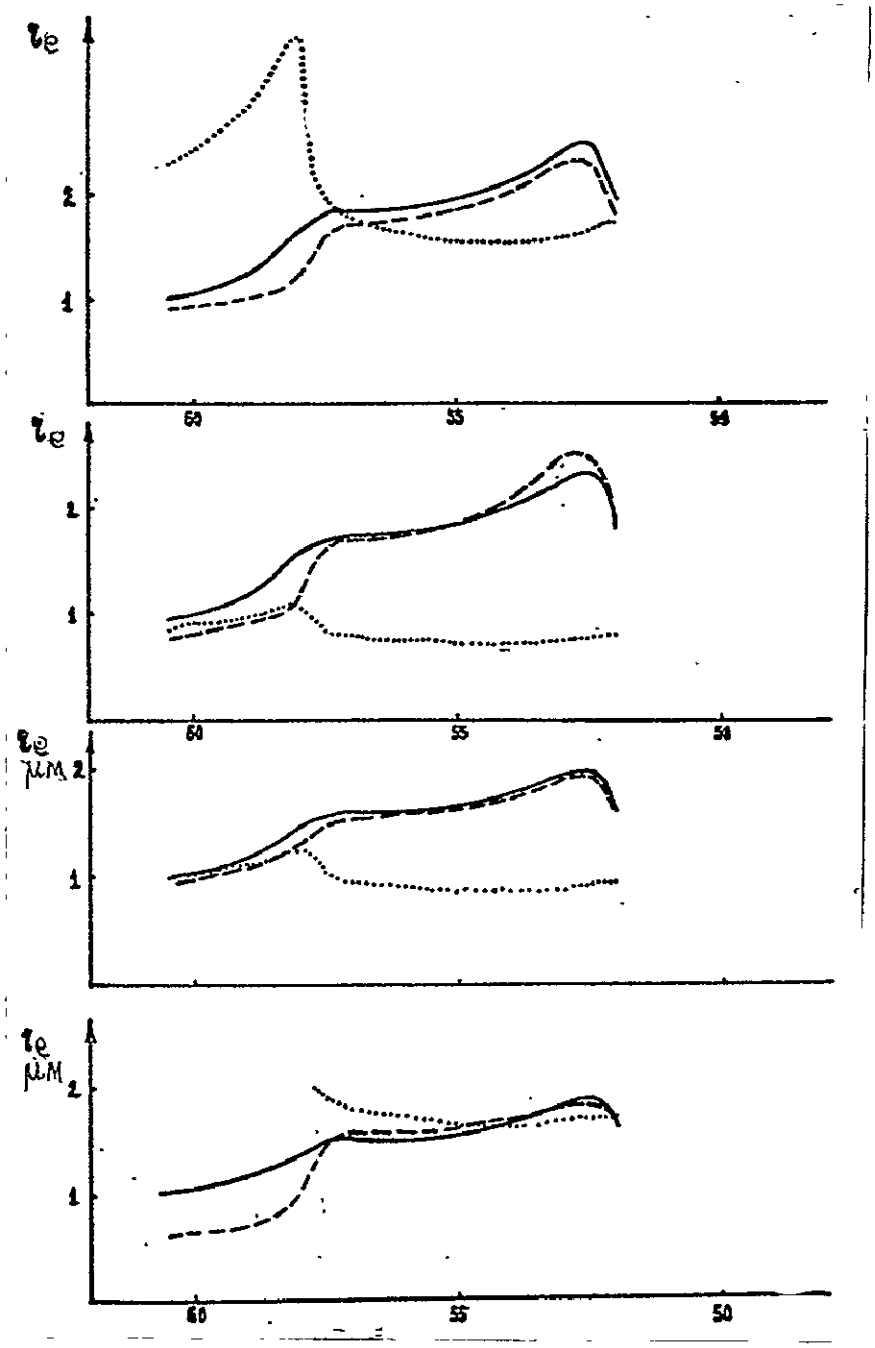

Figs. 19 and (following page) 20. Altitude dependences of $\tau_e^{1,2,3}(h)$, found from the $f^e_{1,2,3}(h)$ values for various models.

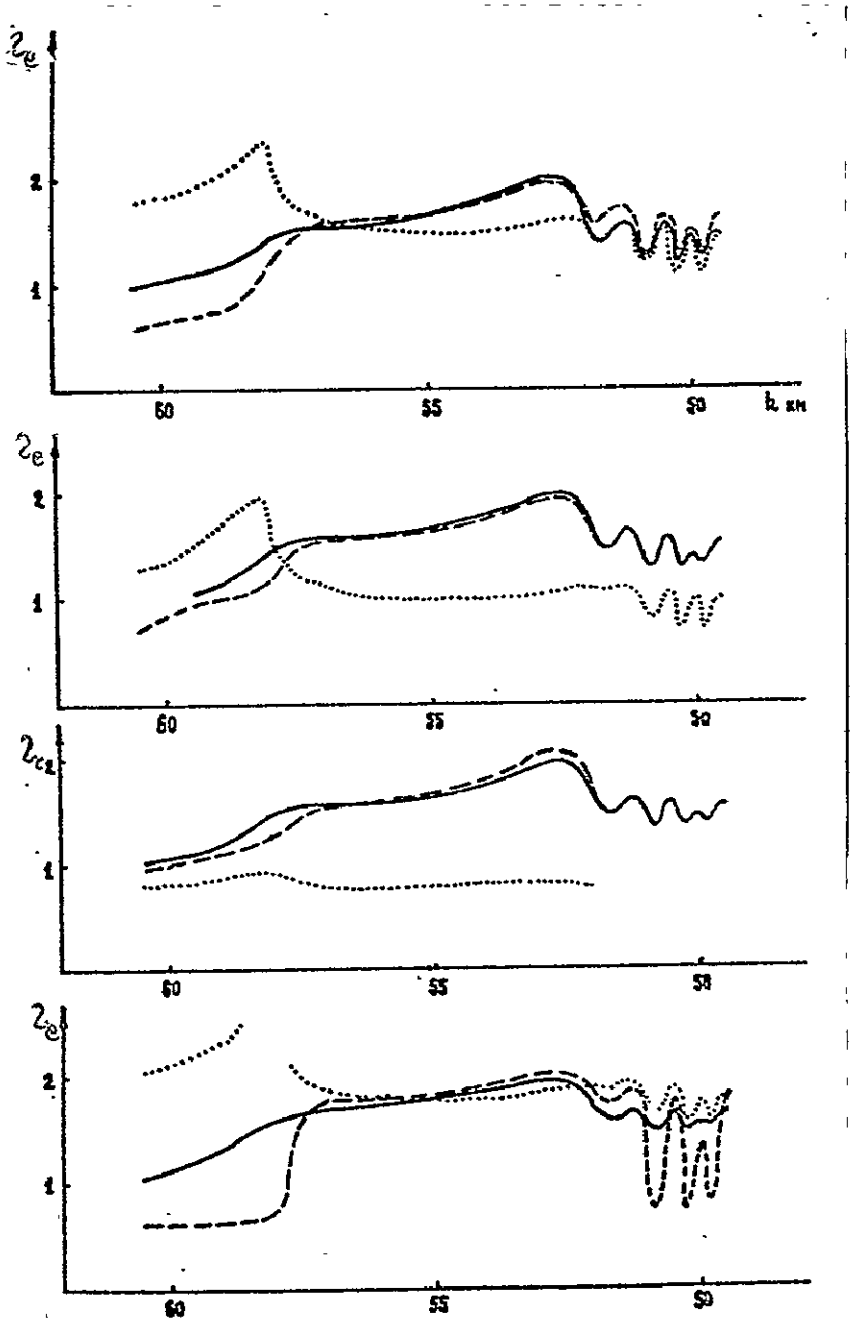

Fig. 20

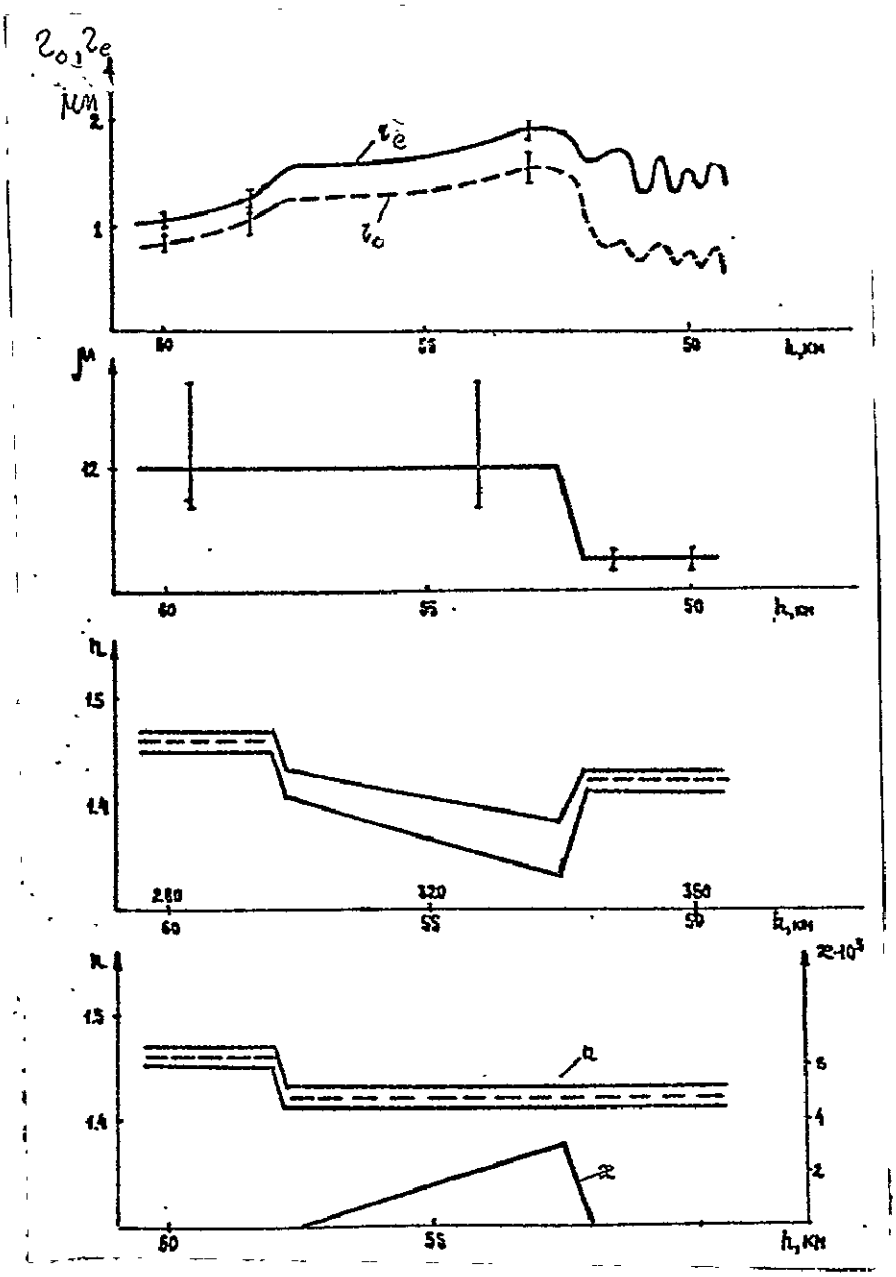

Fig. 21. Microphysical characteristics of cloud aerosols in dependence on the altitude: $\gamma_e(h)$, $\gamma_0(h)$, $n(h)$, and $\mu(h)$.

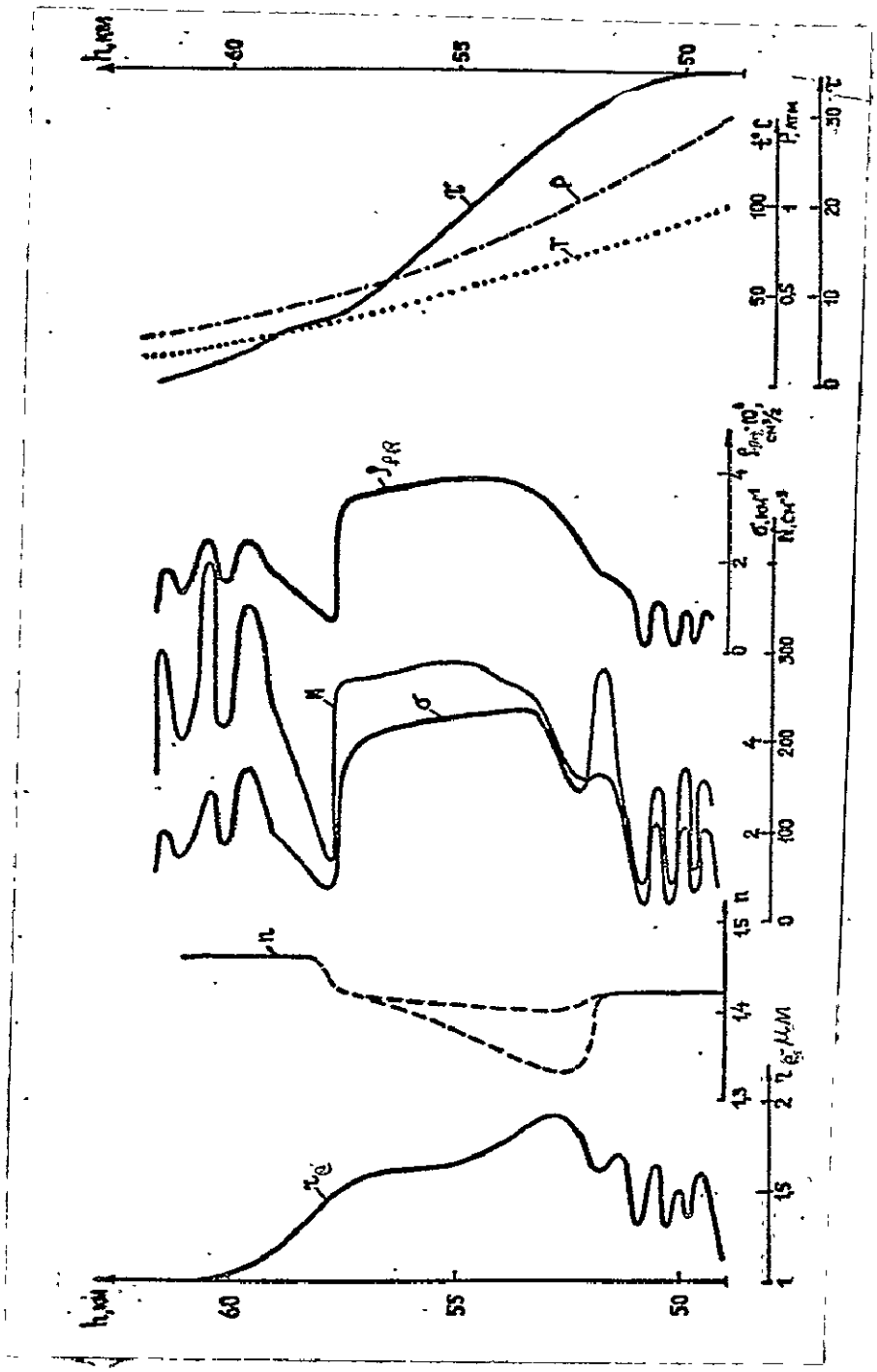

Fig. 22. Altitude profiles for the main optical and structural characteristics of the Venusian clouds, compared with temperature T and pressure P profiles.

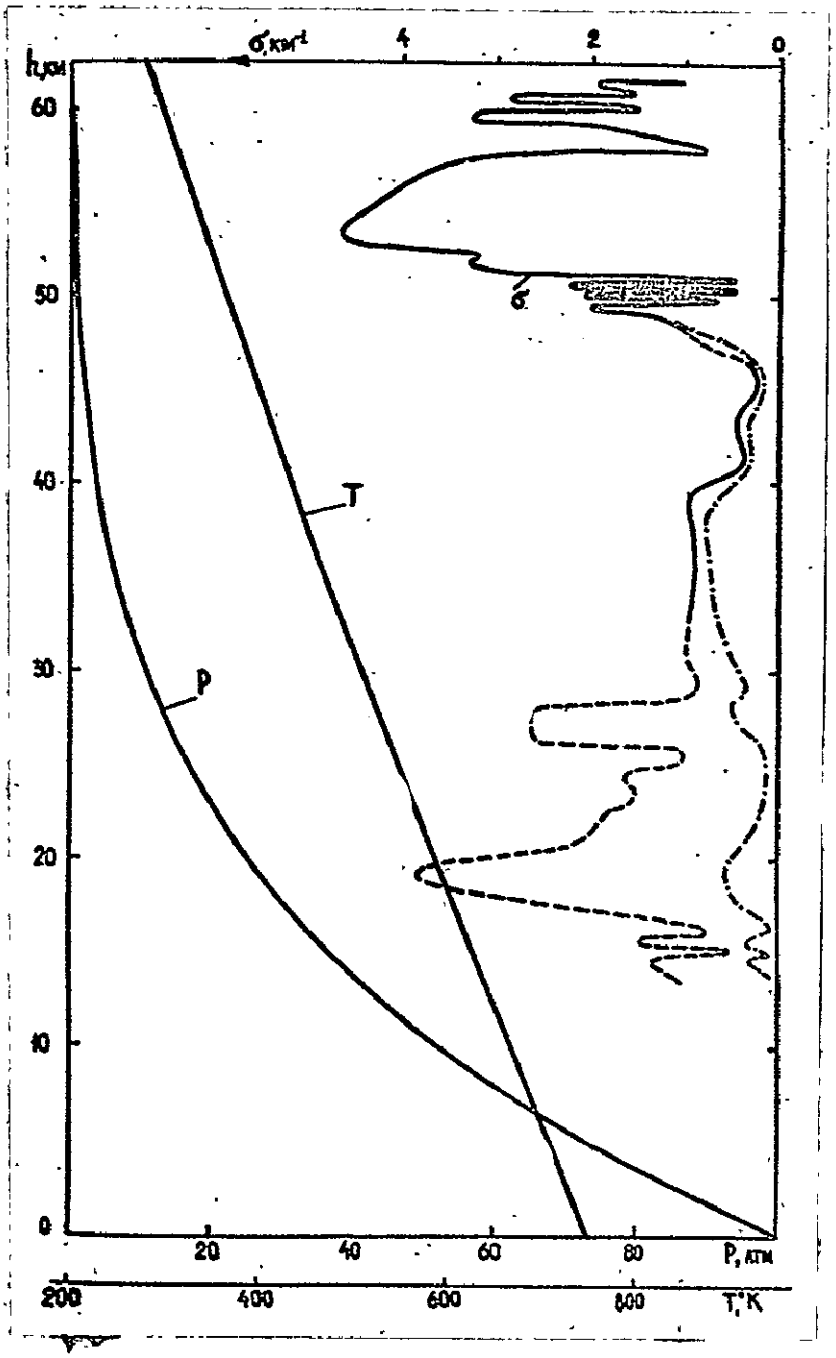

Fig. 23. Optical density of the aerosols, the temperature, and the pressure of the Venusian atmosphere in the altitude range 62-14 km.

REFERENCES

1. Avduyevskiy, V. S., Marov, M. Ya., in Aeromekhanika i gazovaya dinamika (Aeromechanics and gas dynamics), Nauka, Moscow, 1976, p. 205.

2. Avduyevskiy, V. S., Marov, M. Ya., Moshkin, B. Ye., and Ekonomov, A. P., Dokl. AN SSSR, 210, 799, 1973.

3. Avduyevskiy, V. S., Golovin, Yu. M., Zavelevich, F. S., Likhushin, V. Ya., Marov, M. Ya., Mel'nikov, D. A., Merson, Ya. I., Moshkin, B. Ye., Razin, K. A., Chernoshchekov, L. I., Ekonomov, A. P., Kosmich. issled. 14, pp 735-742, (1976).

4. Borovskiy, N. V., and Volkovitskiy, O. A., Trudy IPG, Vol. 7, (1967).

5. Kuz'min, A. D., Marov, M. Ya., Fizika planety Venera (The Physics of the Planet Venus), Nauka, Moscow, (1974).

6. Lukashevich, N. L., Shari, V. P., Preprint #83, IAM USSR AS, (1977).

7. Marov, M. Ya., Ryabov, O.L., Preprint #39, IAM USSR AS, (1972).

8. Marov, M. Ya., Lebedev, V. N., Lystsev, V. Ye., Pis'ma v A. Zh., 2/5, (1976).

9. Marov, M. Ya., Byvshev, B. V., Manuilov, K. N., Baranov, Yu. P., Kuznetsov, I. S., Lebedev, V. N., Lystsev, V. Ye., Maksimov, A. V., Popandopulo, G. K., Razdolin, V. A., Sandimirov, V. A., Frolov, A. M., Kosmich. issledov., 14, p. 729, (1976).

10. Marov, M. Ya., Lebedev, V. N., Lystsev, V. Ye., Kuznetsov, I. S., Popandopulo, G. K., Preprint #44, IAM USSR AS, (1977).

11. Marov, M. Ya., Lebedev, V. N., Lukashevich, N. L., Lystsev, V. Ye., Shari, V. P., Otchet IPM AN SSSR, (1978).

12. Prishnvalko, A. P., Naumenko, Ye. K., Preprint of the I.F. BSSR, Minsk, (1972).

13. Tikhonov, A. N., Arsenin, V. Ya., Metody resheniya nekorrektnykh zadach (Methods of solving improper problems), Nauka, Moscow, 1974.

14. Shari, V. P., Lukashevich, N. L., Preprint #105, IAM USSR AS, (1977).

15. Hansen, J. E., Hovenier, J. W., J. Atm. Sci., 31, p. 1137, (1974).

16. Sill, G. T., Commun. Lunar Planet. Lab., #171, pp. 191-198, (1972).

17. Young, L. D. G., and Young, A. T., Astrophys. J., 197, pp. L39-L43, (1973).

18. Young, A. T., Icarus, 32, pp. 1-26, (1977).